Gondwana Research 79 (2020) 283–300

Contents lists available at ScienceDirect

Gondwana Research

journal homepage: www.elsevier.com/locate/gr

Early central American forearc follows the subduction initiation rule

Scott A. Whattam [a, *], Camilo Montes [b], Robert J. Stern [c]

[a] Department of Geosciences, King Fahd University of Petroleum and Minerals, Dhahran, 31261, Saudi Arabia
[b] Department of Physics and Geology, Universidad del Norte, Barranquilla, Colombia
[c] Department of Geosciences, University of Texas at Dallas, Richardson, TX, USA

ARTICLE INFO

Article history:
Received 12 October 2018
Received in revised form
11 September 2019
Accepted 2 October 2019
Available online 9 November 2019

Keywords:
Central American forearc
Subduction initiation
Subduction initiation rule
Forearc
Volcanic arc
Ophiolite

ABSTRACT

The "subduction initiation rule" (SIR) (Whattam and Stern, 2011) advocates that proto-arc and forearc complexes preserved in ophiolites and forearcs follow a predictable chemotemporal and/or chemostratigraphic vertical progression. This chemotemporal evolution is defined by a progression from bottom to top, from less to more depleted and slab-metasomatized sources. This progression has been recently documented for other igneous suites associated with subduction initiation. The Sona-Azuero forearc complex of southern Panama represents the earliest magmatic arc activity at the Central American Volcanic Arc system. Comparison of new and existing geochemical data for the circa 82-40 Ma Sona-Azuero Proto-Arc/Arc, its underlying 89-85 Ma "oceanic plateau" of SW Panama and the 72-69 Ma Golfito Proto-Arc of southern Costa Rica with the 70-39 Ma Chagres-Bayano Arc of eastern Panama exhibits a chemotemporal progression as described above and which follows the SIR. Sona-Azuero lavas are predominantly MORB-like, whereas those of the younger Chagres-Bayano complex are mostly VAB-like; lavas of the Golfito Proto-Arc typically show characteristics intermediate to that of the Sona-Azuero and Chagres-Bayano proto-arc/arc complexes. On the basis of isotope evidence as shown in other studies, lava types of all three complexes are clearly derived from a source contaminated by the Caribbean Large Igneous Province plume; we term these "plume-contaminated" forearc basalts and volcanic arc basalts, respectively. Apart from a plume-induced subduction initiation origin for the Panamanian forearc, these insights suggest otherwise similar petrogenetic origins and tectonic setting to lavas comprising earliest-formed forearc crust, and most ophiolites, which follow the SIR.

1. Introduction

Ophiolites are ancient, on-land vestiges of oceanic lithosphere ascribed to seafloor spreading to form a nascent proto-forearc in the earliest stages of subduction initiation. As shown by Whattam and Stern (2011), Tethyan-type supra-subuduction zone ophiolites (Pearce et al., 1984; Pearce, 2003) of the Eastern-Mediterranean-Persian Gulf region (Robertson, 2004) exhibit similar chemostratigraphic/chemotemporal progressions (changes in lava chemistry with time) as that of forearc lithosphere of classic records of magmatism during subduction initiation, such as the Izu-Bonin-Mariana intra-oceanic arc system (Reagan et al., 2010; Ishizuka et al., 2011). Tethyan-type ophiolites for example, in Oman (Semail), Greece (Pindos) and Albania (Mirdita) formed by initial eruption of MOR-like tholeiitic basalts (i.e., forearc basalts, FAB, Reagan et al., 2010) followed by calc-alkaline volcanic arc basalt (VAB) or basaltic-andesite lavas and intrusives characterized by large ion lithophile-enrichment and high-field strength element-depletion, which were sometimes followed by latest-stage boninites (e.g., Alabaster et al., 1982; Saccani and Photiades, 2004; Dilek et al., 2008). This exact sequence is not universal but a common theme is emerging from global examples. Variations in subduction initiation progression is revealed by the Troodos ophiolite which lacks MORB-like tholeiites and instead shows a progression from earlier-formed basalt-andesite-dacite-rhyolite series backarc basin-like basalts to boninites (Pearce and Robinson, 2010). At the Izu-Bonin-Mariana forearc, generation of earliest MORB-like FAB during initial subduction initiation was followed by eruption of boninites (Reagan et al., 2010, 2017); from this time forward igneous activity retreated to the site of the long-term magmatic front. A similar chemotemporal progression has recently been documented for the nascent stages of Greater Antilles Arc system construction (Torró et al., 2017). This chemotemporal progression reflects complementary magmatic and mantle responses (MORB → VAB affinities and fertile lherzolite → depleted harzburgite, respectively) during subduction initiation and encapsulates the

* Corresponding author.
E-mail addresses: sawhatta@gmail.com, scott.whattam@kfupm.ed.sa (S.A. Whattam).

https://doi.org/10.1016/j.gr.2019.10.002
1342-937X/

Table 1
Age constraints for the Golfito, Sona-Azuero and Chagres-Bayano complexes. Abbreviations: A, arc; CR, Costa Rica; PA, proto-arc; PAN, Panama; OP, oceanic plateau. Superscripts: a, Azuero Arc includes the proto-arc of Buchs et al. (2010); b, is to indicate that this refers to a restricted segment of the Azuero Arc (the Río Quema Formation, Corral et al., 2011); c, Golfito also consists of basaltic trachyandesite and andesite according to Buchs et al. (2010) and references therein; a TAS plot (not shown) does suggest this, however a plot of Nb/Y vs. Zr/Ti (not shown) suggests that designation of alkaline affinities is the result of alteration (addition of alkalis); d, similarly, the Nb/Y vs. Zr/Ti plot suggests no alkaline affinities; e, Wegner et al. (2011) suggested alteration could account for the high K_2O contents of some rock types which is confirmed by a Nb/Y vs. Zr/Ti plot; f and g, interpreted by Hauff et al. (2000) and Buchs et al. (2010) as oceanic plateau and proto-arc/arc, respectively.

Golfito Complex (i.e.,Proto-Arc, southern Costa Rica)	submarine	?	subalkaline basalt, basaltic trachyandesite, trachyandesite	massive to thin pillowed lava flows	late Campanian to middle Maastrichian (~72-69 Ma)	biostratigraphic fossil ID	oceanic plateau and proto-arc/ arc	Dengo (1962); Schmidt-Effing (1979); Obando (1986); Di Marco (1994); Di Marco et al. (1995);Hauff et al. (2000); Buchs et al. (2010)
Azuero Complex (S. Panama) Azuero Plateau	submarine	?	subalkaline basalt, (minor) gabbro	sheet flows, pillow basalts, rare gabbroic intrusives	Coniacian-Early Santonian (~89–85)	Biostratigraphic fossil (radiolarite) ID	oceanic plateau	Giudice and Recchi (1969); Metti and Recchi (1976); Kolarsky et al. (1995); Hoernle et al., (2002); Lissinna et al. (2002, 2006); Lissinna (2005); Buchs et al. (2009, 2010); Wörner et al., (2009); Corral et al., (2011); Wegner et al., (2011); Montes et al. (2012a)
Azuero Proto-Arc & Arc		~1.7	tholeiitic basalt to rhyolite and their plutonic equivalents (including enriched OIB-like varieties)	lavas flows, dykes, lava domes, large intrusive complexes	Late Cretaceous to Early Maastrichian 82-40	Biostratigraphic fossil (foraminifera) ID; radiometric ($^{40}Ar/^{39}Ar$, LA-ICP-MS U–Pb on zircons)	proto-arc/arc	
Chagres-Bayano Arc (E. Panama)	submarine	~ 3	subalkaline basalt, (minor) gabbro basalt to rhyolite and their plutonic equivalents	massive and pillowed lava flow-dyke complex with associated sub-volcanic plutonic rocks with overlying and intercalated volcaniclastic breccias	70–39	radiometric ($^{40}Ar/^{39}Ar$, LA-ICP-MS U–Pb on zircons)	arc	Maury et al. (1995); Wörner et al. (2005, 2009); Wegner et al., (2011); Montes et al. (2012a, 2012b)

Table 1 Whattam, 2019.

Fig. 1. (a) Present tectonic configuration of the Circum-Caribbean region. (b) Magnification and detail of the boxed region in Fig. 1a showing the distribution of Late Cretaceous to middle Eocene (~75-39 Ma) arc magmatism in Golfito, easternmost Costa Rica, Sona-Azuero, southern Panama and Chagres-Bayano, eastern Panama. Abbreviations in: (a) CR, Costa Rica,; GAA, Greater Antilles Arc; LAA, Lesser Antilles Arc; PAN, Panama; PR, Puerto Rico. (b) CB, Chagres-Bayano; CI, Coiba Island; Cord de Pan, Cordillera of Panama; GF, Golfito; PC, Panama City; PCFZ, Panama Canal Fracture Zone.

'subduction initiation rule' (SIR) of Whattam and Stern (2011). The SIR stipulates that the composition of subduction initiation lavas change from less to more high-field strength depleted and from less to more slab-metasomatized with time, i.e., lavas change from MORB-like to VAB-like over the course of subduction initiation, and this rule links forearcs formed during subduction initiation and ophiolites. This chemotemporal progression evolution reflects formation of proto-forearc/forearc lithosphere as a result of mantle melting that is increasingly influenced by enrichments from the sinking slab during subduction initiation. Mid-oceanic ridge-like FAB lavas are the consequence of decompression melting of upwelling asthenosphere and mark the initial magmatic manifestation of subduction initiation. Contribution of fluids from dehydrating oceanic crust and sediments on the sinking slab is minor during the early stages of subduction initiation, but continuous melting results in a depleted, harzburgitic residue. This residue is increasingly metasomatized by fluids from the sinking slab and later partial melting of this residue yields 'typical' suprasubduction-zone-like lavas with high-field strength element depletions and large ion element enrichments in the latter stages of subduction initiation. Recognizing the SIR has profound implications for the development of robust tectonic plate reconstructions and interpreting and understanding forearc formation during subduction initiation. Identification of the SIR in ophiolite complexes implies formation similar to that of forearc lithosphere via seafloor spreading during subduction initiation (Stern and Bloomer, 1992; Stern et al., 2012).

The purpose of this paper is not to provide a regional treatment of the tectonic evolution of or new stratigraphic constraints on the early Central American forearc but rather, to examine the early Central American forearc as an extension to cases for which the SIR has been tested so far. We do this by focusing on Late Cretaceous and Early Paleogene igneous rocks of Central America and compare their chemotemporal (changes in chemistry with time) progression

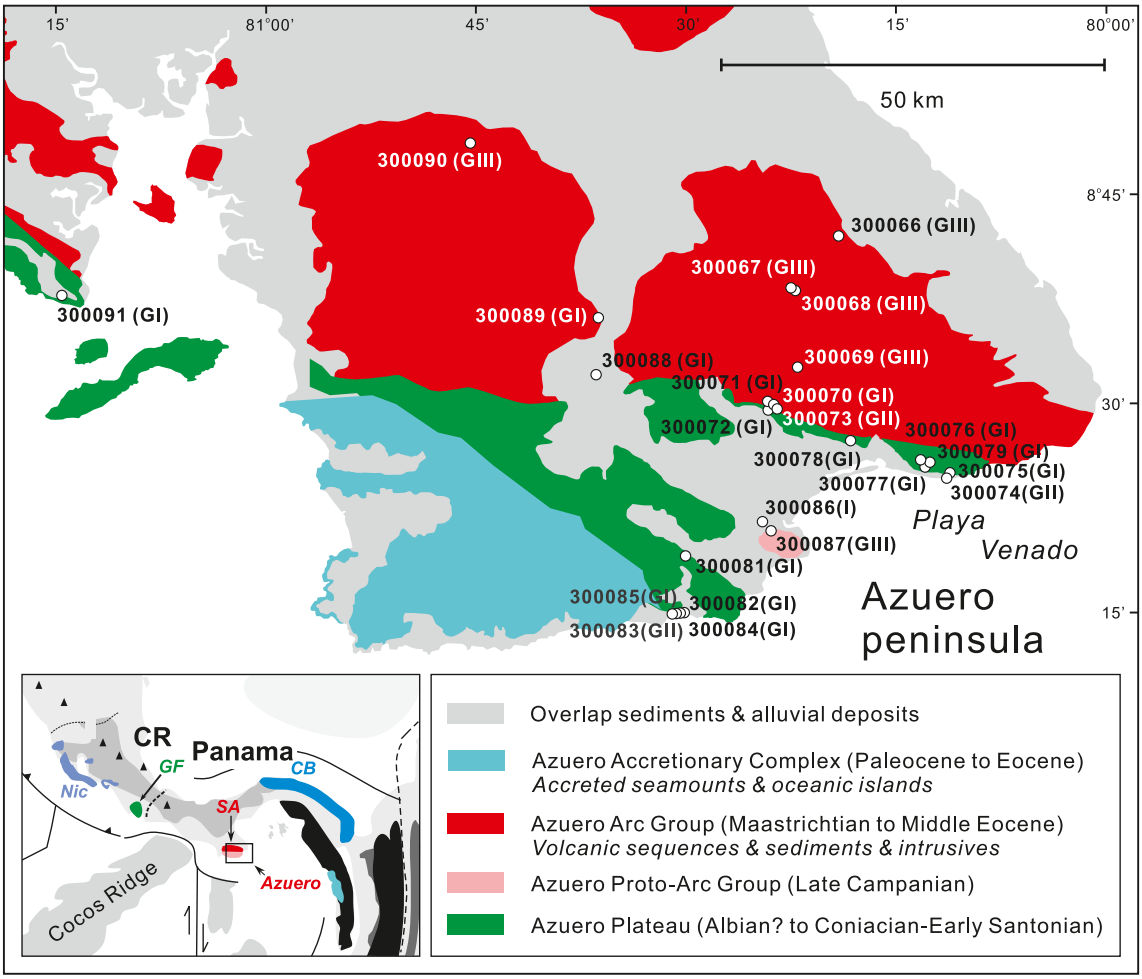

Fig. 2. Geologic map of the Azuero peninsula showing the location of our samples. Map is modified from *Dirección General de Recursos Minerales* (1991), Buchs et al. (2010) and Corral et al. (2011). See Fig. 1 for broader location of the Azuero peninsula. Abbreviations: CB, Chagres-Bayano; G, Group: GI, Group I; GII, Group II; GIII, Group III; Nic, Nicaragua; SA, Sona-AzueroSee text for definitions of these groups.

with the chemotemporal progression of other complexes associated with subduction initiation (forearcs and ophiolites).

Crucial to our chemotemporal arguments is recognition that the Sona-Azuero and Golfito proto-arc/arc segments in central Panama and SW Costa Rica, respectively, began to form at least 5 M.y. prior to establishment of the Chagres-Bayano Arc in central Panama (see Section 2 for Regional setting and the Supplementary Document for description of these complexes). We document the availability of absolute and relative ages which provides the basis of this recognition in the Supplementary Document (Table S1, see also Table 1).

2. Regional setting

As a result of detailed multidisciplinary studies of Late Cretaceous 'oceanic igneous terranes' (terminology of Hauff et al., 1997) and arc-related complexes exposed in the forearc of the Central American Volcanic Arc (Fig. 1a) in Costa Rica (e.g., Buchs et al., 2010) and Panama (Fig. 1b) (e.g., Hauff et al., 2000a; Tomascak et al., 2000; Geldmacher et al., 2001, 2008; Lissinna, 2005; Gazel et al., 2009, 2015; Wörner et al., 2009; Buchs et al., 2009, 2010; Wegner et al., 2011; Montes et al., 2012a, 2012b; Whattam and Stern, 2015a, 2015b) we can re-evaluate the chemotemporal evolution of these oldest Central American Volcanic forearc complexes in the context of subduction initiation processes. Most researchers agree that the bulk of the Caribbean Plate is composed of the Caribbean Large Igneous Province (CLIP) (Fig. 1a), an expansive oceanic "plateau" that formed over the Galapagos hotspot prior to its northeasterly drift and insertion between North and South America (see Kerr et al., 2000) prior to subduction initiation. Relatedly, the CLIP is interpreted by most as underlying younger arc segments not only in Costa Rica and Panama but also along NW South America in western Ecuador and Colombia all the way to the Leeward Antilles in Curaçao and Aruba (see references in Whattam and Stern, 2015a). The 'standard' model holds that volcanic arc construction occurred upon the trailing edge of the CLIP in present-day Costa Rica and Panama (Pindell and Kennan, 2009; Wörner et al., 2009; Buchs et al., 2010; Wegner et al., 2011) and elsewhere in the Caribbean realm along the southern margin of the Caribbean Plate in NW South America and the Leeward Antilles. In contrast, on the basis of collated geochemical, isotopic and radioisotopic age datasets of these 'plume-and-arc-related' complexes in Central America and NW South America which exhibit compositional and temporal overlap between Late Cretaceous hotspot-derived CLIP magmatism and the magmatic effects of subduction initiation, Whattam and Stern (2015a) suggested arc construction in a single, rapidly evolving hybrid plume- and subduction-related environment. By 'plume- and subduction-related' we mean proto-forearc/forearc complexes that were generated synchronously or nearly so as a result of interaction between the plumehead and the (soon to be) subduction-modified lithosphere that it interacted with; as a result, the complexes which constitute this study were generated from a mantle source that was plume-dominated at first and evolved with

Table 2
Whole rock ICP-AES analyzes of Groups I, II, and III Azuero lavas from this study. Abbreviation: bas-and, basaltic-andesite.

Sample No.	300070	300071	300075	300076	300077	300078	300079	300081	*300082*	*300082 (Rep)*	*300084*	*300085*	Sample No.	300086	300088
Lithology	basalt	basalt	basalt	basalt	basalt	basalt	basalt	basalt	*basalt*	*basalt*	*basalt*	*basalt*	Lithology	basalt	basalt
Group[a]	Group I	Group I	Group I	Group I	Group I	Group I	Group I	Group I	*Group I*	*Group I*	*Group I*	*Group I*	Groupa	Group I	Group I
major oxides (wt. %)													major oxides (wt. %)		
SiO_2	49.23	48.92	47.29	47.38	49.70	47.00	46.94	46.87	46.61	46.4	45.11	48.00	SiO_2	47.21	47.93
TiO_2	1.22	1.20	1.22	1.23	1.24	1.22	1.26	1.09	1.22	1.23	0.88	0.95	TiO_2	1.22	1.25
Al_2O_3	13.55	13.42	13.92	13.28	13.67	13.70	14.06	14.03	14.02	13.98	13.39	14.10	Al_2O_3	14.03	16.75
Fe_2O_3	11.76	11.74	12.02	11.58	10.80	11.92	12.12	11.16	11.46	11.53	10.29	10.50	Fe_2O_3	12.12	11.04
MnO	0.18	0.18	0.21	0.23	0.18	0.22	0.23	0.26	0.31	0.30	0.18	0.18	MnO	0.20	0.20
MgO	7.38	8.38	7.26	8.05	7.17	8.13	7.01	8.32	7.84	7.99	8.59	8.40	MgO	8.10	6.40
CaO	10.33	9.91	12.76	12.40	9.72	12.20	12.51	11.96	11.71	11.71	9.83	9.82	CaO	11.78	9.48
Na_2O	3.60	3.29	2.09	2.00	2.98	2.23	2.53	2.30	2.16	2.17	2.31	3.56	Na_2O	2.39	3.29
K_2O	0.16	0.18	0.07	0.07	1.74	0.10	0.09	0.07	0.07	0.08	0.57	0.28	K_2O	0.14	0.67
P_2O_5	0.10	0.10	0.10	0.10	0.10	0.10	0.10	0.09	0.09	0.09	0.07	0.07	P_2O_5	0.10	0.11
LOI	2.20	2.40	2.80	3.40	2.40	2.90	2.90	3.60	4.20	4.20	8.50	3.80	LOI	2.40	2.60
total	99.71	99.72	99.74	99.72	99.70	99.72	99.75	99.75	99.69	99.77	99.72	99.66	total	99.69	99.72
Mg#	56	59	55	58	57	58	54	60	58	58	62	61	*Mg#*	57	54
trace elements (ppm)													*trace elements (ppm)*		
Sc	47	48	48	50	48	51	50	48	50	50	46	47	Sc	47	44
V	328	316	326	331	308	336	324	289	310	314	275	325	V	343	308
Ni	68.1	46.4	76.2	69.6	76.0	69.4	85.5	65.8	66.4	NA	51.5	64.3	Ni	48.0	46.4
Cu	140.4	138.1	143.3	142.8	144.4	140.1	145.8	128.3	138.0	NA	109.7	88.0	Cu	138.3	182.7
Zn	56	67	54	61	60	49	57	50	57	NA	49	36	Zn	56	65
Rb	2.4	2.4	0.7	0.6	18.5	1.1	1.0	0.7	0.7	0.6	1.1	3.0	Rb	1.7	7.3
Sr	233.9	204.8	162.7	118.1	209.4	155.4	108.1	142.2	156.7	158.8	134.9	193.3	Sr	143.2	296.3
Y	21.9	21.6	22.7	22.6	20.6	22.4	22.0	18.7	19.9	20.8	16.0	19.0	Y	23.0	23.8
Zr	59.2	58.7	84.1	61.8	57.0	58.2	56.7	66.1	52.4	63.1	41.8	43.1	Zr	59.1	68.4
Nb	3.3	3.9	3.6	3.7	3.3	3.2	3.0	2.9	3.3	3.1	3.2	2.4	Nb	3.6	3.3
Cs	<0.1	<0.1	<0.1	<0.1	<0.1	<0.1	<0.1	<0.1	<0.1	<0.1	<0.1	<0.1	Cs	0.1	0.3
Ba	37	50	14	15	204	17	17	60	27	31	18	151	Ba	60	140
La	3.2	3.6	3.2	3.3	2.8	3.1	3.0	2.6	2.8	2.9	2.3	2.5	La	3.2	3.3
Ce	8.4	8.7	8.7	8.7	7.7	7.7	8.0	6.8	7.6	7.4	5.6	7.2	Ce	9.1	8.7
Pr	1.37	1.4	1.42	1.41	1.32	1.35	1.34	1.14	1.22	1.24	0.97	1.04	Pr	1.42	1.39
Nd	7.5	7.3	7.1	7.4	6.5	7.5	7.0	5.9	6.4	6.6	5.1	6.4	Nd	7.1	7.4
Sm	2.4	2.35	2.51	2.47	2.19	2.35	2.23	1.99	2.17	2.11	1.62	1.93	Sm	2.14	2.41
Eu	0.90	0.91	0.97	0.92	0.90	0.92	0.89	0.79	0.89	0.89	0.63	0.72	Eu	0.99	0.92
Gd	3.18	3.25	3.39	3.40	2.97	3.24	3.17	2.75	3.03	2.96	2.27	2.44	Gd	3.14	3.37
Tb	0.63	0.63	0.64	0.64	0.59	0.62	0.60	0.54	0.57	0.58	0.44	0.49	Tb	0.61	0.65
Dy	3.78	3.80	3.76	3.86	3.77	3.90	3.92	3.24	3.49	3.54	2.71	3.22	Dy	3.66	4.22
Ho	0.80	0.82	0.82	0.83	0.79	0.82	0.77	0.69	0.74	0.73	0.59	0.67	Ho	0.85	0.89
Er	2.34	2.37	2.44	2.41	2.30	2.40	2.35	2.04	2.06	2.15	1.69	2.00	Er	2.62	2.68
Tm	0.36	0.36	0.36	0.35	0.35	0.37	0.36	0.31	0.33	0.31	0.26	0.29	Tm	0.34	0.39
Yb	2.28	2.36	2.30	2.33	2.35	2.30	2.33	1.97	2.15	2.25	1.84	1.79	Yb	2.29	2.55
Lu	0.35	0.36	0.36	0.35	0.34	0.33	0.34	0.30	0.33	0.33	0.26	0.27	Lu	0.34	0.39
Hf	1.9	2	2.3	2.0	2.0	1.8	1.8	2.0	1.7	1.5	1.2	1.3	Hf	1.8	1.9
Ta	0.2	0.2	0.2	0.3	0.2	0.2	0.2	0.2	0.3	0.1	0.1	0.2	Ta	0.2	0.2
Pb	0.6	0.2	0.6	0.2	0.2	0.3	0.3	0.2	<0.1	NA	0.1	<0.1	Pb	0.3	0.2
Th	0.3	<0.2	0.3	0.2	0.4	<0.2	0.2	<0.2	<0.2	0.2	0.2	<0.2	Th	<0.2	0.4
U	0.1	0.1	0.1	0.2	0.1	0.1	0.1	<0.1	0.1	0.1	<0.1	<0.1	U	<0.1	0.1

Major element detection limits are about 0.001–0.4%. Other notes: Samples Group numbers in italics are samples with total oxide concentrations <96 wt % and which were thus excluded from our chemical plots (see Section 4.3.2.).
NA = Not analyzed. Rep = Replicate (analysis). STD = Standard.
Table 2 Whattam, 2019.
[a] Group refers to classification on the basis of petrographic characteristics (see Supplementary Document) and trace element chemistry (see Section 5.1 and Supplementary Document).

time to be modified by subduction. According to this model, arc formation occurred subsequent to subduction initiation which was catalyzed by plume emplacement (plume-induced subduction initiation). A plume-induced subduction initiation mechanism has recently been shown to be valid on the basis of numerical thermomechanical modelling (Gerya et al., 2015).

Although the Farallon Plate has been subducting beneath the western Americas since at least 200 Ma, subduction initiation at the Central American Arc was independent of Farallon Plate subduction. Central America subduction initiation began between 90 and 75 Ma along the western periphery of the Caribbean Large Igneous Province (CLIP), which was emplaced within the middle of the Farallon Plate beginning about 92 Ma (Sinton et al., 1997; Kerr et al., 2003 and references therein). Some previous studies of the Central American forearc igneous complexes discussed in this study (see Supplementary Document] suggest that subduction initiation began ~75-71 Ma with the magmatic arc growing on pre-existing oceanic plateau (CLIP) basement (Buchs et al., (2010); Wegner et al., (2011))_. In contrast, Lissinna et al. (2006) suggest that the infant Panamanian island arc on the western side of the CLIP dates back to 89 Ma. The studies of Lissinna et al. (2006) and Wegner et al. (2011) did not posit a cause for subduction initiation but Buchs et al. (2010) suggested this was tectonically induced, caused by compression of the thickened Caribbean Plate during westward migration of the Americas and collision with South America. As explained above, Whattam and Stern (2015a) in contrast suggested that subduction initiation was the result of plume emplacement and discuss why an induced subduction

300089 basalt Group I	300091 basalt Group I	300072 basalt Group II	300073 basalt Group II	300074 basalt Group II	*300083 basalt Group II*	300066 andesite Group III	300067 basalt Group III	300068 basalt Group III	Sample No. Lithology Groupa	*300069 bas-and Group III*	*300087 basalt Group III*	300090 basalt Group III	STD SO-18	STD SO-18 Rep 1	STD SO-18 Rep 2	STD SO-18 Rep 3
major oxides (wt. %)									major oxides (wt. %)							
48.78	47.04	44.77	43.97	46.95	45.00	56.28	48.11	47.06	SiO_2	54.30	47.40	50.34	58.29	58.22	58.13	58.11
1.76	1.26	4.55	4.69	2.76	3.64	1.14	0.57	0.51	TiO_2	0.19	1.74	0.44	0.7	0.7	0.69	0.69
13.72	13.86	11.78	11.82	13.34	13.09	15.37	20.30	18.78	Al_2O_3	11.39	14.29	18.34	13.98	13.98	14.11	14.13
13.18	11.74	16.96	16.68	14.18	13.37	9.05	8.79	10.11	Fe_2O_3	11.49	12.70	10.06	7.59	7.59	7.58	7.58
0.21	0.21	0.23	0.21	0.22	0.17	0.17	0.15	0.19	MnO	0.19	0.22	0.20	0.4	0.4	0.39	0.39
6.23	7.55	5.52	5.46	6.51	5.62	3.46	4.91	7.24	MgO	7.40	5.85	5.28	3.34	3.35	3.35	3.33
10.80	12.64	8.34	11.06	9.82	9.46	6.37	10.80	12.99	CaO	7.84	8.85	9.80	6.31	6.35	6.36	6.38
2.74	1.80	3.46	2.15	3.25	3.86	3.94	3.23	1.63	Na_2O	2.20	3.49	2.25	3.71	3.7	3.7	3.71
0.17	0.04	0.46	0.51	0.33	0.92	0.99	0.47	0.10	K_2O	0.29	1.14	0.32	2.15	2.16	2.15	2.16
0.18	0.10	0.44	0.45	0.24	0.43	0.31	0.07	0.05	P_2O_5	0.07	0.17	0.10	0.83	0.84	0.82	0.81
2.00	3.50	3.20	2.70	2.10	4.20	2.80	2.40	1.10	LOI	4.30	3.80	2.60	1.9	1.9	1.9	1.9
99.77	99.74	99.71	99.70	99.70	99.76	99.88	99.80	99.76	total	99.66	99.65	99.73	99.76	99.76	99.74	99.74
48	56	39	39	48	46	43	53	59	*Mg#*	56	48	51	47	47	47	47
trace elements (ppm)									*trace elements (ppm)*							
53	48	38	38	39	28	31	33	43	Sc	59	44	41	26	26	25	25
351	309	462	463	426	336	193	241	296	V	338	336	267	192	191	205	207
17.3	73.6	34.8	34.6	51.1	56.0	2.3	16.3	9.9	Ni	20.3	19.2	9.1	46	45	46	43
100.1	135.4	317.7	323.7	140.9	25.1	42.4	151.5	221.6	Cu	71.7	107.8	118.1	NA	NA	NA	NA
64	52	139	107	88	75	57	40	17	Zn	128	75	35	NA	NA	NA	NA
1.2	0.4	5.0	7.1	4.5	16.5	11.6	7.2	2.1	Rb	3.2	14.5	8.2	26.4	26.4	27.8	28
146.0	172.0	72.7	155.9	218.3	473.0	229.5	373.7	360.7	Sr	164.8	336.9	764.3	377.8	380.7	399	413.7
37.4	21.4	51.2	53.4	32.0	29.5	31.7	11.6	10.7	Y	8.8	32.9	13.5	29	29.7	31.3	31.4
105.0	63.3	272.2	281.5	141.1	237.6	101.9	25.5	11.0	Zr	15.0	100.2	25.6	261.1	264	278.9	282.7
2.2	3.8	20.3	20.9	12.0	32.7	3.3	1.2	0.8	Nb	1.8	2.5	0.5	18.9	19.1	19.4	20.5
<0.1	<0.1	<0.1	<0.1	<0.1	<0.1	<0.1	0.3	0.1	Cs	<0.1	<0.1	0.1	6.5	6.7	6.7	7
71	12	51	59	92	140	397	159	72	Ba	668	1100	219	476	484	500	513
4.2	3.3	17.4	17.7	9.8	23.4	10.9	2.6	2.3	La	3.2	5.0	3.4	11.2	11.4	12.1	12.2
12.0	8.2	45.7	46.8	24.5	55	24.0	5.6	4.6	Ce	4.9	13.8	6.9	24.7	25.2	26.9	27.5
2.13	1.36	6.87	7.31	3.77	7.27	3.51	0.89	0.73	Pr	0.90	2.32	1.16	3.15	3.16	3.27	3.31
12.6	7.1	34	34	18.1	33	16.4	4.2	3.4	Nd	4.2	12.2	5.9	13.1	12.7	13.6	13.4
4.00	2.28	9.23	9.74	5.33	7.21	4.28	1.29	1.28	Sm	1.05	3.65	1.62	2.73	2.71	2.84	2.84
1.41	0.88	2.83	2.91	1.85	2.39	1.37	0.57	0.58	Eu	0.35	1.42	0.57	0.81	0.84	0.84	0.84
5.44	3.15	10.75	10.94	6.21	7.47	5.23	1.74	1.69	Gd	1.24	4.87	2.03	2.77	2.8	2.95	2.94
1.04	0.62	1.76	1.83	1.06	1.11	0.89	0.33	0.32	Tb	0.22	0.90	0.34	0.48	0.47	0.5	0.49
6.42	3.75	10.06	10.05	6.07	6.00	5.63	2.02	1.91	Dy	1.26	5.70	2.13	2.74	2.73	2.86	2.88
1.38	0.78	1.84	1.97	1.20	1.05	1.16	0.44	0.42	Ho	0.28	1.18	0.48	0.58	0.58	0.6	0.61
4.11	2.29	5.02	5.22	3.24	2.80	3.43	1.32	1.19	Er	0.85	3.48	1.44	1.71	1.7	1.71	1.79
0.62	0.34	0.68	0.71	0.47	0.37	0.51	0.21	0.20	Tm	0.15	0.52	0.23	0.27	0.26	0.27	0.27
4.03	2.22	4.36	4.65	3.07	2.39	3.51	1.31	1.29	Yb	1.05	3.40	1.54	1.63	1.69	1.73	1.74
0.59	0.32	0.60	0.62	0.42	0.33	0.50	0.20	0.20	Lu	0.18	0.50	0.24	0.27	0.26	0.26	0.27
3.1	1.8	7.7	8.5	4.0	6.3	3.1	0.9	0.4	Hf	0.5	2.5	0.9	8.8	9	9.2	9.6
0.1	0.3	1.5	1.3	0.8	2.1	0.2	<0.1	<0.1	Ta	<0.1	0.1	<0.1	6.8	6.9	6.9	7.2
0.8	0.3	1.1	1.1	0.6	2.1	1.8	1.1	1.3	Pb	2.3	0.4	1.3	NA	NA	NA	NA
0.3	0.2	1.5	1.3	0.8	1.8	1.9	0.5	<0.2	Th	0.3	0.5	0.4	9.9	9.9	10.4	10.1
<0.1	<0.1	0.5	0.6	0.4	0.5	0.6	0.2	<0.1	U	0.2	0.1	0.2	15.3	15.4	15.8	16.1

initiation scenario was unlikely (see Section 5.4; see also Section 5.5 for a discussion of different subduction initiation mechanisms). We note that the timeframe of the Whattam and Stern (2015a) model, which posits subduction initiation as the result of plume emplacement at 90 Ma, is consistent with the conclusions of Lissinna et al. (2006) who suggest subduction initiation by 89 Ma.

The active Central American volcanic front stretches ~1100 km along the western margin of the Caribbean plate from Costa Rica through Nicaragua, El Salvador and Guatemala to the Guatemala-Mexico border at the southern margin of the North American plate (Fig. 1a). The locus of magmatic activity has shifted from east to west after the Eocene. Early plume- and subduction related sequences in the east comprise the ~89-40 Ma Sona-Azuero (Azuero Marginal Complex of Buchs et al., 2010), 72-69 Ma Golfito, and 70-39 Ma Chagres-Bayano complexes (Fig. 1b, see also Table 1, Table S1 and the Supplementary Document for description of these complexes). The Sona-Azuero and Chagres-Bayano complexes are interpreted as being floored by the 89-85 Ma CLIP (Wörner et al., 2009; Buchs et al., 2010; Wegner et al., 2011; Montes et al., 2012a, 2012b) and the Golfito Complex has been interpreted as both CLIP oceanic plateau (Hauff et al., 2000) and more recently as arc (Buchs et al., 2010). Prior to the study of Buchs et al. (2010), it was generally assumed that most oceanic forearc units along western Costa Rica and Panama represented uplifted segments of the CLIP. Similar interpretations have been made for many oceanic complexes along NW South America and the Leeward Antilles (see Whattam and Stern, 2015a).

3. Methods

3.1. Petrography

Fifty new representative thin sections of the Sona-Azuero complex lavas were examined under a petrographic microscope. Sample locations and coordinates are provided in Fig. 2 and Table S2, respectively, and selected micrographs comprise Supplementary Fig. S1.

3.2. Elemental analysis

Whole-rock samples (n = 25) of the Azuero complex were crushed and ground to powders for major, trace and rare earth element determinations (Table 2). Details of analytical procedures and elemental analysis are provided in the Supplementary Document.

3.3. Data compilation and manipulation

3.3.1. Data compilation

For comparison with our 25 new whole-rock geochemical analyses of Azuero lavas (Table 2), we also compile geochemical data of lavas of the Sona-Azuero (Buchs et al., 2010; Wegner et al., 2011), Golfito (Hauff et al., 2000; Buchs et al., 2010) and Chagres-Bayano complexes (Wegner et al., 2011; Montes et al., 2012b). For further comparison with these Central America forearc complex datasets, we also compile data of global MORB (Gale et al., 2013) and volcanic arc basalts (VAB) of depleted arc systems (PetDB, https://www.earhchem.org/petdb and GEOROC, (http://georoc.mpch-mainz.gwdg.de/georoc/; see Hawkesworth et al., 1997, for definition of 'depleted arc systems'); Late Cretaceous to Eocene 'plume and arc related' units (Whattam and Stern, 2015a) in Panama and Costa Rica; lavas from complexes around the circum-Caribbean region interpreted as CLIP; SIR ophiolite lavas (Whattam and Stern, 2011); Izu-Bonin forearc basalts (Reagan et al., 2010; Shervais et al., 2019; and Izu-Bonin 'forearc-like' basalts (Arculus, 2015)). The MORB dataset (Gale et al., 2013) is mostly basalt (mean of 50.4 wt % SiO2) but ranges from 44.9 to 70.4 wt % SiO2. Volcanic and plutonic samples comprising Late Cretaceous to Eocene (~85-39 Ma) 'plume and arc-related' units (Whattam and Stern, 2015a) in Panama and southernmost Costa Rica are considered as either oceanic plateau or proto-arc and arc constructed upon the CLIP (e.g., Buchs et al., 2010) or hybrid plume- and arc-related (Whattam and Stern, 2015a). Basalts interpreted as CLIP (n = 192 tholeiitic and 7 enriched oceanic-island-like basalts) are compiled from GEOROC and are from the Caribbean Sea; the western margin of the Caribbean Plate in Costa Rica (Nicoya, Herradura, Tortugal); the western margin of NW South America in western Ecuador (Piñón Formation and the Pallatanga and Pedernales-Esmeraldas unit) and western Colombia (Gorgona Island, Serrania de Baudo Formation and the Western Cordillera); the Lesser Antilles in Aruba (Aruba Lava Formation); and the Caribbean Sea (Colombian and Venezuelan Basins).

3.3.2. Data manipulation

In order to assure that suitable quality analyses of least altered samples of Sona-Azuero, Golfito and Chagres-Bayano were used in our study, only samples which yield oxide totals of 96–102 wt % (excluding loss on ignition, LOI) are plotted. In our geochemical plots using major elements, oxides are recalculated on an anhydrous (volatile-free) basis and normalized to 100%. However, our geochemical plots and arguments rely primarily on trace elements known to be non-mobile up to greenschist-facies metamorphic conditions.

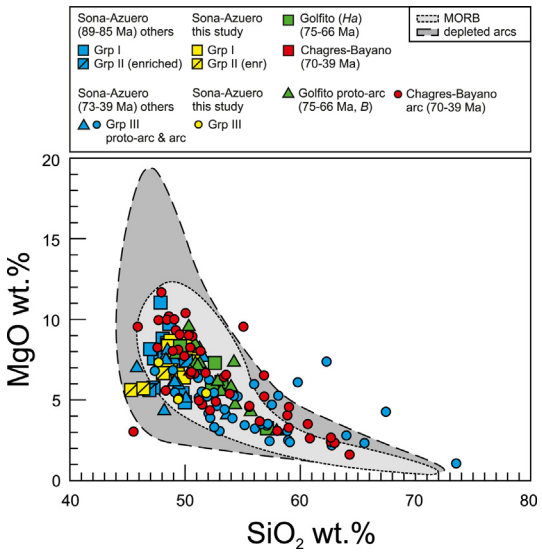

Fig. 3. MgO vs. SiO_2 for all lavas of this study superimposed with the fields of MORB and lavas of depleted arc systems (see text). Abbreviation: enr, enriched.

4. Results

Our lavas are subdivided into three chemical groups on the basis of chondrite-normalized La/Yb concentrations (see section 4.2.1 and Fig. 5). Groups I, II and III are analogous to those interpreted by others as plateau basalts, (volumetrically subordinate) enriched basalts and proto-arc or arc basalts (Buchs et al., 2010; Wegner et al., 2011), respectively. As shown by Wegner et al. (2011) and Whattam and Stern (2015a,b), Group I are tholeiitic, Group III range from tholeiitic to calc-alkaline and Group II are analogous to oceanic island tholeiites (Supplementary Fig. 2).

4.1. Petrography

Most Group I MORB-like (see Section 5) Azuero lavas are fine-grained tholeiitic basalts. Textures are typically intergranular to intersertal or subophitic and mineralogy is primarily plagioclase, clinopyroxene and alteration products (Supplementary Fig. S1a, b). In other very fine-grained varieties, clinopyroxene is not obvious and the mineralogy is dominated by thin, wispy, highly altered plagioclase laths. Other samples are coarser-grained and some of these, with large, sericitized plagioclase laths and fresh, subhedral, interstitial clinopyroxene, are texturally similar to Group III arc-like (see Section 5) basalts. The crystallization sequence of plagioclase followed by clinopyroxene is typical of MORB (Bryan, 1983; Pearce et al., 1984).

Group II oceanic island basalt-like (see Section 5, Supplementary Fig. S1c, d) lavas are subordinate, making up ~10–20% of the total Azuero samples in our dataset and the combined datasets of Buchs et al. (2010) and Wegner et al. (2011). Overall, these basalts are moderately to heavily altered and distinguished by their chocolate brown coloration and ubiquitous calcite- and chlorite-filled amygdales in the coarser-grained, weakly porphyritic and medium-grained plagioclase phyric samples. Fine-grained varieties of these basalts exhibit micro-porphyritic texture defined by ~1 mm clinopyroxene and 2–5 mm plagioclase phenocrysts. Apatite is an accessory phase (typically <5%).

Our Group III arc-like (see Section 5) Azuero lavas are rare (n = 3) and in contrast to lavas of Groups I and II, usually display micro-porphyritic or unique to this group, robustly porphyritic textures defined by large (1.5–2.0 mm), commonly euhedral, fresh

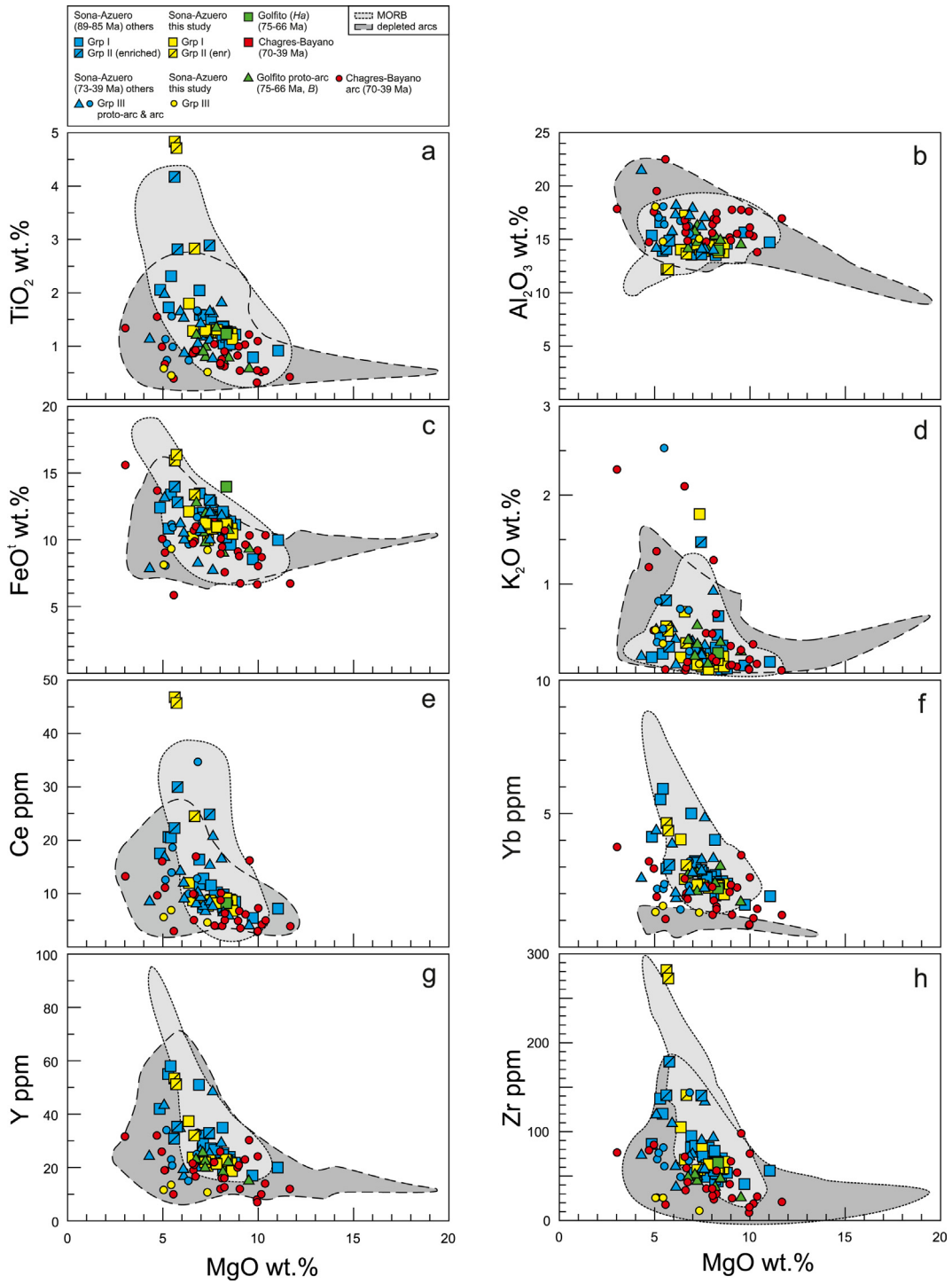

Fig. 4. MgO vs. (a) TiO2, (b) Al2O3, (c) FeOt, (d) K2O, (e) Ce, (f) Yb, (g) Y and (h) Zr for all lavas of this study superimposed with the fields of lavas of MORB and depleted arc systems (basalts only)Abbreviation: enr, enriched.

clinopyroxene phenocrysts (Supplementary Fig. S1e, f). The crystallization sequence, in contrast to the Group I MORB-like lavas, is clinopyroxene followed by plagioclase which is typical of hydrous (i.e., arc) magmas in which early plagioclase crystallization is suppressed (Pearce et al., 1984; Cameron 1985; Sisson and Grove 1993).

4.2. Major element chemistry

4.2.1. MgO vs. TiO_2, Al_2O_3, FeO^t and K_2O

As developed below in Section 4.3, the Sona-Azuero lavas of Buchs et al. (2010), Wegner et al. (2011) and our dataset are subdivided into three groups on the basis of chondrite-normalized La/Yb concentrations. Group I are interpreted by Buchs et al. (2010) and Wegner et al. (2011) as plateau basalts; Group II as enriched basalts (Buchs et al., 2010); and Group III as proto-arc or arc volcanics (Buchs et al., 2010; Wegner et al., 2011). These groupings are referred to below.

A plot of SiO_2 vs. MgO (Fig. 3) shows that lavas considered in this study range from basaltic to rhyolitic with MgO concentrations of 1.06–11.68 wt%. Fractionation patterns for MORB ($n = 14, 782$) and

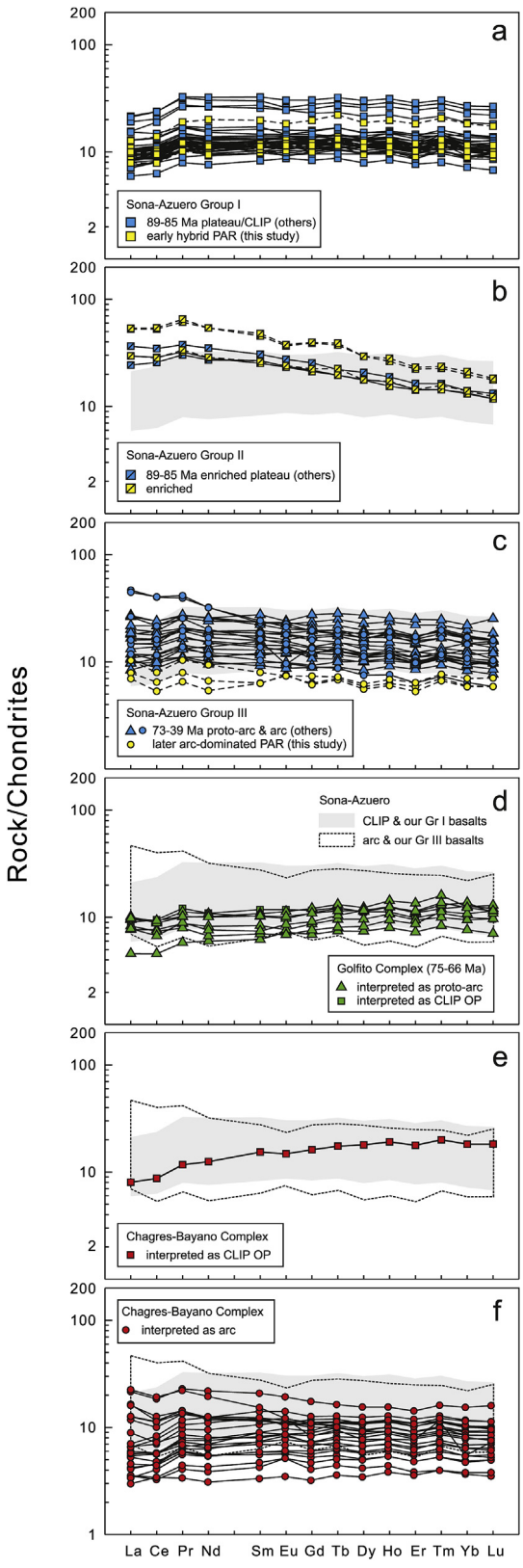

Fig. 5. Chondrite-normalized REE-normalized plots of Sona-Azuero lavas with 52 or less wt. SiO_2 from this study vs. Sona-Azuero, Golfito and Chagres-Bayano lavas with less than 52 wt % SiO_2 from other studies. The similarity in chondrite-normalized LREE fractionations, i.e., $[La/Yb]_{CN}$ of our samples with those from other studies (Lissinna, 2005; Buchs et al., 2010; Wegner et al., 2011) in (a–c) form the basis for classification of our samples into three groups (see Table 3 for further details): (i) Group I, LREE-depleted, (ii) Group II, LREE-enriched (transitional to alkalic) and (iii) Group III, flat to slightly LREE-enriched. Chondrite concentrations are from Nakamura (1974).

depleted (see Hawkesworth et al., 1997) arc systems ($n = 4,379$) are broadly similar but with the latter ranging to lower MgO at low SiO_2 contents (˂55 wt%) and higher MgO at higher SiO_2 (55–72 wt%). Despite the considerable overlap of MORB and VAB, a large number of Sona-Azuero Group III arc ($n = 8$) and Chagre-Bayano samples ($n = 7$) exhibit higher arc-like MgO than MORB at silica concentrations ˃ 55 wt% SiO_2. As well, two Sona-Azuero proto-arc, three Sona-Azuero Group II samples (including two from this study) and one Chagres-Bayano sample display lower SiO_2 than MORB for a given MgO concentration at low SiO_2 (45–48 wt %) and fall within the arc domain.

In Fig. 4a–d, we plot MgO vs. TiO_2, Al_2O_3, FeO^t and K_2O for basalts of our Azuero dataset alongside basalts of the Sona-Azuero, Golfito and Chagres-Bayano suites. For comparison, also plotted on Fig. 4 are lavas of MOR and depleted arc systems (basalts only). In all plots there exists considerable overlap between MORB and VAB but some samples plot uniquely within either field. In consideration of MgO vs. TiO_2, all six Sona-Azuero Type II basalts plot uniquely within or just above the MORB field and outside of the arc field. Two of our three Type II Sona-Azuero basalts also have Al_2O_3 and FeO^t concentrations which plot within the MORB field. In MgO vs. TiO_2 and the remainder of the MgO vs. major oxides plots (Al_2O_3, FeO^t and K_2O), between two to four low-magnesium (~3–6 wt% MgO) Chagre-Bayano lavas plot uniquely within the arc field. Similarly, apart from K_2O, one low MgO (~4.2 wt% Mg) Sona-Azuero proto-arc sample plots distinctively within the arc field; two of our Sona-Azuero Type III arc lavas have TiO_2 and FeOt akin to arc basalts. Additionally, two high MgO (~10–12 wt %) Chagre-Bayano lavas exhibit MgO vs. TiO_2, Al_2O_3, FeO^t and K_2O compositions that plot distinctly within the arc field or on the cusp between MORB and arc. The remainder of samples plot within the overlapping area between MORB and VAB.

4.3. Trace element chemistry

4.3.1. MgO vs. Ce, Yb, Y and Zr

We also plot MgO vs. a light and heavy rare earth element (LREE, Ce and HREE, Yb) and two high field strength elements (Y, Zr) for basalts of our Azuero dataset alongside basalts of the Sona-Azuero, Golfito and Chagres-Bayano suites for comparison with MORB and depleted arc system basalts (Fig. 4e–h). In terms of MgO vs. Ce, two of our Sona-Azuero high-TiO_2 Group II samples plot above both the MORB and arc fields with the highest Ce of all samples (46–47 ppm) whereas two Sona-Azuero Group II samples of Buchs et al. (2009) plot within the MORB field along with one Sona-Azuero proto-arc and arc sample. Many low-magnesium (˂6 wt% MgO) basalts plot within the arc field including two of our Sona-Azuero Group III arc lavas, three Sona-Azuero Group I lavas interpreted as plateau by Buchs et al. (2009) and Wegner et al. (2011), three Sona-Azuero Group III arc basalts and five Chagres-Bayano basalts. On the other end of the MgO spectrum, one high-MgO (~11 wt % MgO) Group I Sona-Azuero and one Chagres-Bayano basalt (~12 wt % MgO) also plot within the arc field. The remaining basalts plot where the MORB and arc fields overlap in MgO vs. Ce space.

On a plot of MgO vs. Yb (Fig. 4f), four Sona-Azuero Group III arc basalts including all three of our Sona-Azuero Group III basalts plot alongside six Chagres-Bayano basalts uniquely within the low-HREE arc field. Also, three Sona-Azuero Group I, six Sona-Azuero Group III proto-arc and arc and six Chagre-Bayano basalts plot outside of both the MORB and arc field; the remaining majority of

Abbreviations: OP, oceanic plateau; PAR, plume- and arc-related. The grey region in (b) to (f) represent the data presented in (a) and the dashed regions in (d) to (f) represent the data presented in (c).

samples plot within the MORB realm with Yb ˃ ~1.4.

Many samples exhibit arc-like HFSE concentrations. On a MgO vs. Y plot (Fig. 4g), our three Sona-Azuero Group III basalts, four of six Sona-Azuero Group II basalts and eight Sona-Azuero Group III proto-arc and arc basalts fall alongside almost half of the Chagre-Bayano basalts (12 of 26 samples) within the arc field. Our three Sona-Azuero Group III basalts and Chagres-Bayano basalts exhibit the lowest Y concentrations (˂14 ppm). The remaining basalts fall within an area of MORB and arc overlap. A similar trend is seen on MgO vs. Zr (Fig. 4h) with our Sona-Azuero Group III and Chagres-Bayano basalts exhibiting the lowest Zr arc-like contents of all samples.

4.3.2. Subdivision of Sona-Azuero lavas into three groups on the basis of $[La/Yb]_{CN}$

Table 3 provides the foundation for subdivision of our Azuero lavas into three groups on the basis of chondrite-normalized La/Yb concentrations ($[La/Yb]_{CN}$).

Compositionally, our Azuero Group I basalts are slightly to moderately light rare earth element depleted ($[La/Yb]_{CN} = 0.75–1.09$, mean = 0.96) and compositionally analogous to the Group I (non-enriched) Azuero 'plateau' samples of Buchs et al. (2010) and the 'CLIP' basalts of Wegner et al. (2011) ($[La/Yb]_{CN} = 0.63–1.15$, mean = 0.92, Table 3).

Our Group II Azuero basalts are volumetrically subordinate, light rare earth element-enriched ($[La/Yb]_{CN} = 2.29–2.86$) and compositionally similar to the Group II 'enriched plateau' samples of Buchs et al. (2010) ($[La/Yb]_{CN} = 1.92–2.81$) (Table 3). Taking all enriched samples into consideration (i.e., of Buchs et al., 2010 and ours), these basalts are perhaps best described as oceanic island tholeiites (OIT on Supplementary Figure 2) on the basis of TiO_2 vs. Y/Nb relations (Floyd and Winchester, 1975; Winchester and Floyd, 1977).

On the basis of chondrite-normalized rare earth element and N-MORB-normalized plots (see below), our Group III lavas are VAB-like and analogous to the Azuero Proto-Arc and Arc samples of Buchs et al. (2010) and the 'CLIP' Arc samples of Wegner et al. (2011), although our samples range to lower absolute rare earth element concentrations. Rare earth element patterns of Group III lavas range from slightly light rare earth element-enriched ($[La/Yb]_{CN} = 1.28–1.58$], Table 3) to flat to slightly 'U-shaped' (see next section), i.e., middle rare element-depleted, e.g., two samples have $[La/Gd]_{CN} > 1$ and $[Yb/Gd]_{CN} > 1$).

4.3.3. Chondrite-normalized rare earth element and N-MORB-normalized incompatible element plots

Chondrite-normalized rare earth element and N-MORB-normalized plots of Sona-Azuero, Golfito and Chagres-Bayano basalts are provided in Figs. 5 and 6, respectively.

Table 3
Mean and range of La/Yb normalized to chondrite ($[La/Yb]_{CN}$) of our Group I, II and III Sona-Azuero lavas vs. Sona-Azuero lavas of other studies (Buchs et al., 2010; Wegner et al., 2011). Chondrite abundances normalized to are from Sun and McDonough (1989).

Group	mean $[La/Yb]_{CN}$	Our data range	*n*	mean [La/Yb]CN	Others range	*n*
I	0.96	0.75–1.09	12	0.92	0.63–1.15	36
II	2.63	2.29–2.86	3	2.39	1.96–2.81	3
III	1.43	1.28–1.58	3	1.43	0.76–3.21	17

Notes: The Group I of others comprise the Azuero and Sona 'CLIP' basalts of Wegner et al., (2011) and the Group I Azuero Plateau basalts of Buchs et al., [2010]; the Group II of others comprise the Group II basalts of Buchs et al. (2010); the Group III of others comprise arc basalts of Azuero, Sona and Coiba Island of Lissinna (2005) and the basalts of the proto-arc and arc of Buchs et al., (2010). Chondrite abundances are from Sun and McDonough (1989).
Table 3 Whattam 2019.

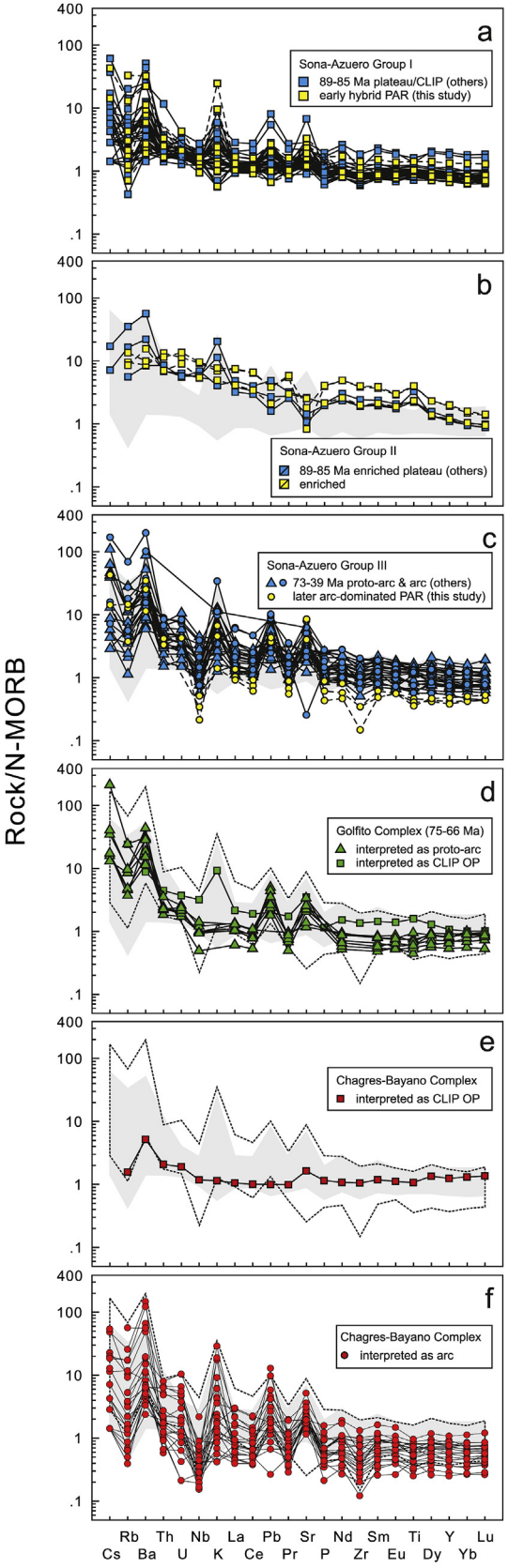

Fig. 6. N-MORB-normalized plots of Sona-Azuero lavas with 52 or less wt. SiO_2 from this study vs. Sona-Azuero, Golfito and Chagres-Bayano lavas with less than 52 wt % SiO_2 from other studies. N-MORB abundances are from Sun and McDonough (1989). Abbreviations: (a, e) PAR, plume- and arc-related; (g, i) OP, oceanic plateau. The grey region in (b) to (f) represent the data presented in (a) and the dashed regions in (d) to (f) represent the data presented in (c).

Although the rare earth element patterns of Golfito and Chagres-Bayano basalts are similar to those of Sona-Azuero there are some significant differences. Rare earth element patterns of proto-arc lavas of the Golfito Complex (Fig. 5d) generally fall within the range of the Group I and Group III Sona-Azuero lavas interpreted as oceanic plateau and proto-arc/arc respectively, but range to very low absolute rare earth element abundances (mean $\sum$ rare earth element of 32) and light rare earth element fractionations (e.g., $[La/Yb]_{CN}$ of 0.81). These values are higher only than that of the Chagres-Bayano Arc (mean $\sum$ rare earth element ~30) and the lone Chagres-Bayano basalt interpreted as oceanic plateau ($[La/Yb]_{CN}$ of 0.47) (Fig. 5e and f). Relatedly, this $[La/Yb]_{CN}$ ratio of the lone Chagres-Bayano basalt interpreted as oceanic plateau (0.47) is much lower than that of the mean of Sona-Azuero oceanic plateau and arc basalts (with mean $[La/Yb]_{CN}$ of 0.93 and 1.54, respectively). Although the Chagres-Bayano Arc exhibits mean $[La/Yb]_{CN}$ intermediate to that of the Sona-Azuero oceanic plateau and proto-arc/arc (mean $[La/Yb]_{CN}$ of 1.18 vs. 0.93 and 1.54, respectively), the absolute rare earth element abundances of Chagres-Bayano Arc lavas range to much lower concentrations (mean $\sum$ rare earth elements of 30) of ~ 3× chondrite (Fig. 5f).

In terms of N-MORB-normalized incompatible element patterns, the most conspicuous differences between our Azuero Groups are: the lack of large ion lithophile element enrichment in fluid-mobile elements (e.g, Rb, Ba, K, Pb) in Group II, which is well developed in both Groups I and III; the lack of a negative Nb-anomaly (with respect to Th and Ce) in Groups I and II, but which is obvious in Group III; and the pattern of Y and the heavy rare earth elements (Yb, Lu), which are flat in Groups I and III but which decrease with decreasing incompatibility in Group II (Fig. 6a–c). The differences between the N-MORB-normalized patterns of the Sona-Azuero basalts interpreted as CLIP plus our Group I basalts interpreted as segments of the earliest hybrid, plume-dominated unit and basalts interpreted as arc are modest, apart from the prominent Nb depletion and the slightly more, fluid-modified compositions of the latter. For example, although the CLIP basalts exhibit no obvious negative Nb-depletion, they do exhibit modest negative Zr and Ti anomalies and contain only slightly less Ba and Pb (Fig. 6a).

N-MORB normalized plots of Golfito and Chagres-Bayano basalts are provided in Fig. 6d–f. Golfito proto-arc basalts fall completely within the range of Sona-Azuero oceanic plateau and proto-arc/arc basalts but range to lower concentrations of large ion lithophile elements (Ba, K, Pb and Sr) (Fig. 6d). Although a negative Nb anomaly is not well developed in the lone Golfito sample interpreted as oceanic plateau (Hauff et al., 2000) it does exhibit a subtle negative Zr anomaly and concentrations of U, Pb, K and Sr higher than or similar to Golfito basalts interpreted as arc (Buchs et al., 2010); the Golfito proto-arc samples of Buchs et al. (2010) exhibit subtle but clear negative Nb anomalies (Fig. 6d)). The N-MORB-normalized incompatible element plot of the lone Chagres-Bayano sample interpreted as oceanic plateau (Fig. 6e) is somewhat anomalous as it lacks the high LILE enrichments exhibited by most other arc (e.g., Chagres-Bayano Arc, Fig. 6f) and oceanic plateau samples.

5. Discussion

In the following sections, we explore the significance of our new geochemical data and that of other workers to address the following questions: (1) Do Late Cretaceous – Paleogene igneous rocks of Panama and Costa Rica follow the "subduction initiation rule" promulgated for the Izu-Bonin-Mariana arc and many ophiolites?; (2) What is the nature of the contact between "oceanic plateau" and arc and chemotemporal evolution of magmatism?; and (3) What was the nature of the early arc system?

5.1. Evidence of adherence of the early central American volcanic arc system to the subduction initiation rule

We focus here on elements that are not mobilized by hydrothermal alteration and metamorphism for the purpose of constraining mantle source fertility, degrees of partial melting and mantle source fugacity. Ratios of Zr/Y, Nb/Y (and Nb/Yb) are useful as these decrease with mantle depletion and as partial melting increases. Because of the compatibility of Y and Yb in garnet, these ratios can also reflect if garnet was present during melt generation but this may be the case only in Group II enriched oceanic island tholeiite-like basalts which exhibit low Y and heavy rare earth element relative to middle rare earth element (Fig. 5b). In Figs. 7–9, in addition to plotting Panamanian and Costa Rican samples from this study, we also plot SIR ophiolite basalts and basaltic andesites for comparison. We do this because SIR ophiolite lavas are (i) thought to have formed during SI in a proto-forearc environment and show a distinctive chemotemporal (change in chemistry with time) trend from less-to more-depleted and subduction–modified compositions with time (i.e., MORB- to VAB-like) (Whattam and Stern, 2011) which (ii) along with other chemical criteria (see below), are critical for understanding the evolution of the mantle sources for Sona-Azuero and Chagres-Bayano.

5.1.1. Source fertility

In Fig. 7, we plot Zr vs Zr/Y. As demonstrated by Whattam and Stern (2011) and shown in Fig. 7a, whereas the older lavas of the earliest-formed lower subduction initiation rule ophiolite units are mostly MORB-like (84% of the lower unit basalts plot as MORB), those of the younger, uppermost unit in contrast plot completely within the VAB field.

These relations show that forearc units progress from tapping/melting of a less to more depleted source or lower to higher degrees of partial melting over the course of seafloor spreading during subduction initiation. Notably, all tholeiiitic Group I Sona-Azuero basalts interpreted as CLIP (Fig. 7b) plot within the compositional field defined by all (Group III) Sona-Azuero and most Chagres-Bayano and Golfito basalts interpreted as proto-arc (Fig. 7c) suggesting a similar source or degrees of partial melting for Sona-Azuero oceanic plateau and arc. As well, Fig. 7c confirms what was shown by the N-MORB and rare earth element plots, i.e., that Chagres-Bayano arc basalts were derived from a more depleted source, or one that has undergone higher degrees of partial melting than Sona-Azuero. Similarly, the Golfito basalts exhibit evidence of derivation from a source intermediate in composition to that of Sona-Azuero and Chagres-Bayano and Sona-Azuero Group III basalts are more similar in composition to Sona-Azuero Group I than to Chagres-Bayano. Geochemical relations demonstrate a MORB to VAB transition from the Sona-Azuero to the Chagres-Bayano unit and demonstrate adherence to the SIR for the early Central American Volcanic forearc.

5.1.2. Degrees of partial melting

Fig. 7 shows that the source(s) of the Chagres-Bayano basalts and our Group III Azuero basalts were either more depleted or underwent higher degrees of partial melting than the Sona-Azuero source. These plots however, don't distinguish between the two possibilities, and if the latter is accurate, provide estimates of the relative degrees of partial melting.

Cr vs. Y (Fig. 8) can be used to determine relative degrees of partial melting of basalts (Murton 1989). Superimposed on Fig. 8 are sources 1, 2 and 3 (S1, S2, S3) which represent a MORB source, a more depleted source after 20% MORB extraction, and a most depleted source after ~12% extraction of S2, respectively. We caution that the F values discussed below are model dependent and we are interested not in absolute degrees of partial melting but

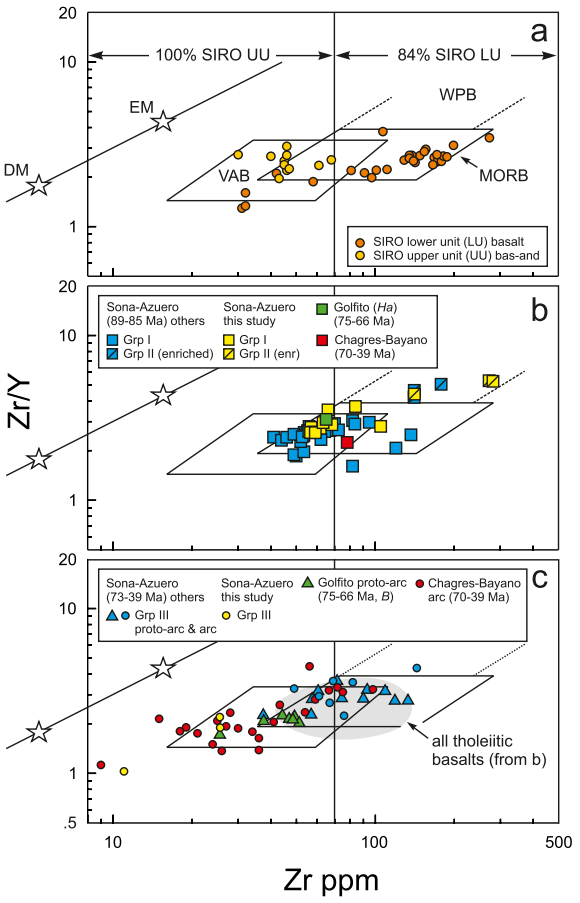

Fig. 7. Zr vs. Zr/Y (Pearce and Norry, 1979) relations of (a) subduction initiation rule ophiolite (SIRO) basalts, (b) Sona-Azuero, Golfito and Chagres-Bayano basalts interpreted as oceanic plateau and our Group I and II Azuero basalts and (c) Sona-Azuero, Golfito and Chagres-Bayano basalts interpreted as arc and our Group III Azuero basalts. All Central American samples are basalts only (i.e., no intrusives). Abbreviations in: (a) bas-and, basaltic andesite; DM, depleted mantle; EM, enriched mantle; WPB, within-plate basalts. (b) *Ha*, Hauff et al. (2000). (c) *B*, Buchs et al. (2010).

differences in partial melting between lavas of Sona-Azuero and Chagres-Bayano. Also shown in Fig. 8a are fields defined by MORB, VAB and boninite (Pearce, 1983). Inspection of Fig. 4b reveals that whereas the lower basalts of subduction initation rule ophiolites are consistent with ~20–40% partial melting of S1 or 20% partial melting of S1 and ~10% partial melting of S2, the upper unit basaltic andesites of subduction initation rule ophiolites indicate higher degrees of partial melting (~10–40% partial melting of S2). A similar relation is seen for Sona-Azuero vs. Chagres-Bayano lavas (Fig. 8c and d). Most Sona-Azuero basalts interpreted as oceanic plateau plot within the MORB field and are consistent with ~20–40% partial melting of S1 (Fig. 8c). Approximately half of the Sona-Azuero basalts interpreted as arc and some Chagres-Bayano arc basalts also plot within the MORB field consistent with ~ up to 40% partial melting of S1, or perhaps more realistically~ 12% melting of S2 (Fig. 8d). The other half of the Sona-Azuero basalts interpreted as arc along with the Golfito basalts record partial melting estimates of 10–20% of S2. Compared to SI ophiolites, the Chagres-Bayano Arc basalts clearly exhibit evidence of derivation from the highest degrees of partial melting. About 35% of the Chagres-Bayano arc basalts plot within the boninite field and are consistent with derivation via up to about 16–17% partial melting of S3. Although boninites require >52 wt% SiO_2, >8 wt% MgO and <0.5 wt% TiO_2 according to the IUGS (Le Bas, 2000), some of these Chagres-Bayano basalts which plot as boninite contain >8 wt% MgO and <0.5 wt% TiO_2 (e.g., samples P-010223-6, PAN-03-016, Wegner et al., 2011).

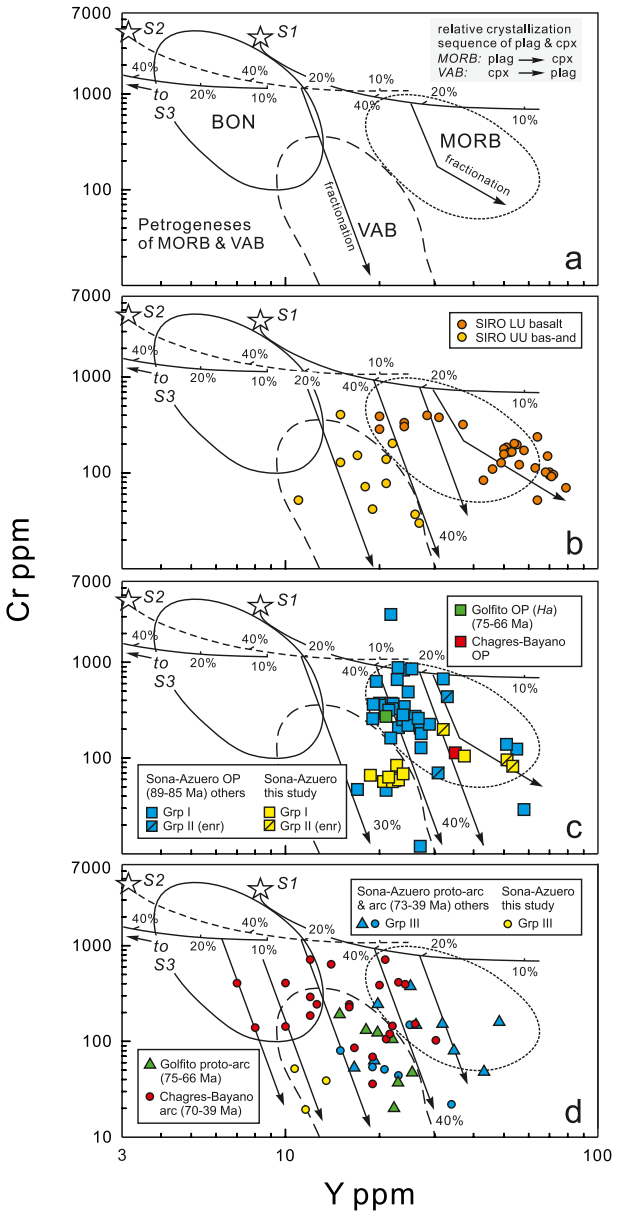

Fig. 8. (a) General petrogenetic paths followed by MORB and VAB and fields of MORB, VAB and boninite (BON) in Y vs. Cr space and Y vs. Cr of (b) subduction initation rule ophiolite basalts, (c) basalts of the Sona-Azuero, Golfito and Chagres-Bayano complexes interpreted as oceanic plateau and our Groups I and II Azuero basalts and (d) arc basalts of the Sona-Azuero, Chagres-Bayano and Golfito complexes and our Group III Azuero basalts (only, no intrusives). All Central American samples are basalts only. The solid and dashed curves represent incremental batch melting trends and source 1 (S1) and source 2 (S2) represent source compositions from Murton (1989). S1 represents a calculated plagioclase lherzolite MORB source comprised of 0.60 oli +0.20 opx +0.10 cpx and S2 represents the residue (residual source) subsequent to 20% melt extraction from S1. The fields of MORB, VAB and within-plate basalt (WPB) are from Pearce (2008) and the boninite (BON) field is from Dilek et al. (2007). Abbreviations in: (b) bas-and, basaltic andesite; LU, lower unit; SIRO, subduction initiation rule ophiolite; UU, upper unit. (c) enr, enriched; *Ha*, Hauff et al. (2000).

Such high degrees of partial melting reflect exceptionally hot and shallow forearc mantle beneath young intra-oceanic subduction-related systems (e.g., Tatsumi and Eggins, 1995). Like the Zr vs Zr/Y plot (Fig. 7) the Cr/Y plot (Fig. 8) demonstrates an unequivocal chemotemporal evolution that follows the SIR.

5.1.3. Source oxygen fugacity

It has long been recognized that MORB are distinguishable from VAB on the basis of Ti/V due to the more oxidized nature (lower Ti/V

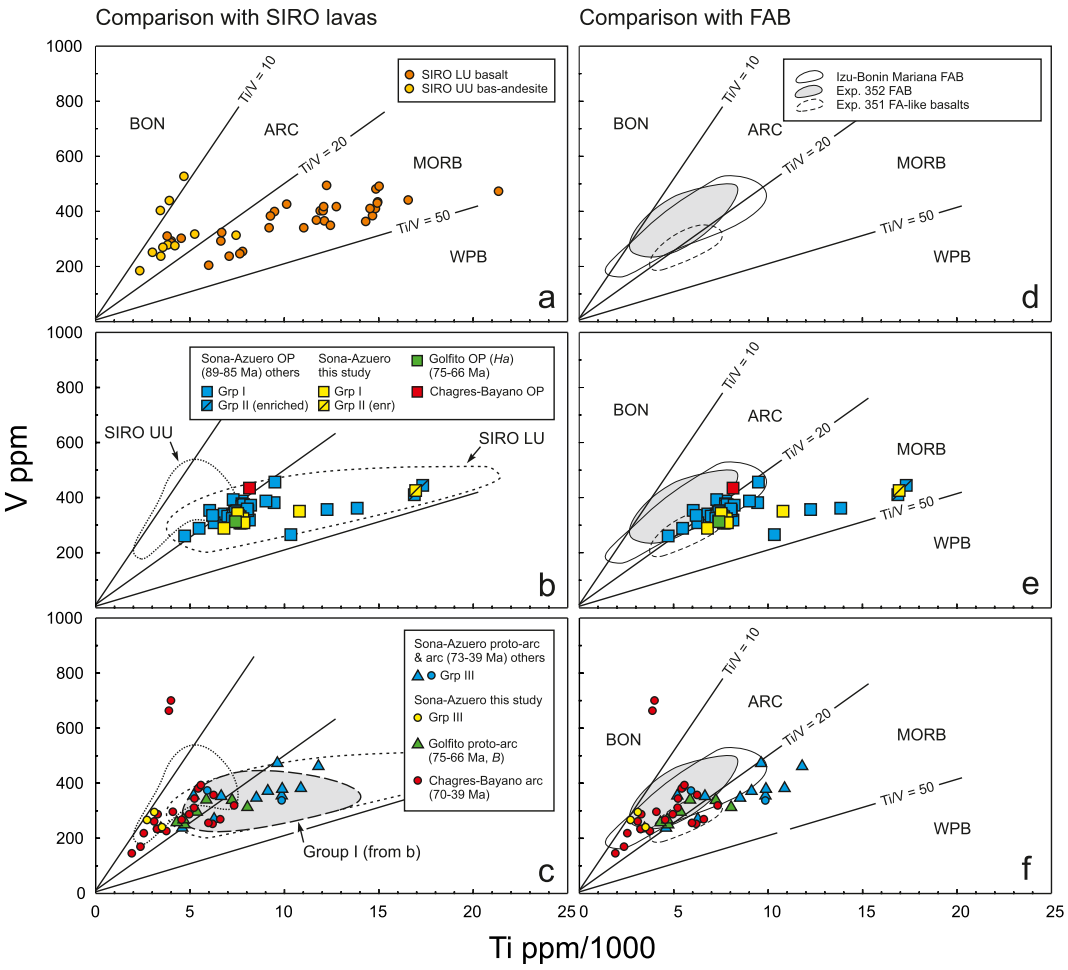

Fig. 9. Ti/V (Shervais, 1982) of (a) subduction initiation rule ophiolite (SIRO) basalts, (b) Sona-Azuero, Golfito and Chagres-Bayano basalts interpreted as oceanic plateau and our Groups I and II Azuero basalts and (c) Sona-Azuero, Golfito and Chagres-Bayano basalts interpreted as arc and our Group III basalts. All Central American samples are basalts only (i.e., no intrusives). Note that two of our enriched Sona-Azuero basalts fall off the plot to the right with 4.7–4.8 wt % TiO_2 (~28000–29000 ppm Ti) and ~460 ppm V (Ti/V of ~53) in Fig. 9b, e within the within-plate basalt field. The Izu Bonin Mariana FAB and Expedition 352 FAB are from Reagan et al. (2010) and Shervais et al. (2019), respectively and the Expedition 351 FA-like basalts are from Arculus (2015). Abbreviations in: (a) BON, boninite; LU, lower unit, UU, upper unit. (b) alk, alkaline; *Ha*, Hauff et al. (2000); LU, UU, as in (a). (c) *B*, Buchs et al. (2010).

ratio) of arc environments vs. the more reduced nature of MORB sources (Shervais, 1982). We plot SIR ophiolite lavas vs. the older and younger segments of the Sona-Azuero, Chagres-Bayano and Golfito complexes in Ti/V space in Fig. 9a–c to demonstrate that the features developed above in various incompatible and immobile elements hold true when considering source fugacity; i.e., whereas the older Sona-Azuero suite (basalts interpreted as oceanic plateau and proto-arc/arc) is consistent with derivation from a MORB-like source, basalts from Chagres-Bayano on the other hand are clearly more consistent with derivation from a more arc-like source.

In Fig. 9d–f, we also plot FAB from the Izu-Bonin Mariana Arc system (Reagan et al., 2010), Exp. 352 forearc basalts from the outer Izu-Bonin Mariana Arc system (Shervais et al., 2019), and Exp. 351 Site U1438 (Arculus, 2015) forearc basalt-like lavas (which presently occupy the rear arc of the Izu-Bonin Mariana Arc system). Lowermost basalts of the Izu-Bonin Mariana forearc were first interpreted as trapped Phillipine Sea Plate (DeBari et al., 1999), a similar interpretation of which was applied to the Tonga forearc (Meffre et al., 2012). However, these first-formed lavas (forearc basalt) are MORB-like and instead mark the first magmatic expression of subduction initiation (Reagan et al., 2010). As shown in Fig. 9e, the vast majority of the older MORB-like Sona-Azuero and the lone Chagres-Bayano basalt (all considered as oceanic plateau) and Golfito basalts plot within the fields defined by the forearc basalts. Similarly, the vast majority of the younger Chagres-Bayano Arc basalts also plot within the field defined by forearc basalts (Fig. 9f), whereby most (77%) of the older Sona-Azuero basalts interpreted as arc plot outside the fields defined by Izu-Bonin Mariana (Ishizuka et al., 2006; Reagan et al., 2010) and Exp. 352 forearc basalts (Expedition 352 Scientists, Preliminary Report, 2015) within the MORB field. This again demonstrates a SIR chemotemporal evolution from early MORB-like lavas to later arc-like lavas, this time on the basis of oxygen fugacity, in the early Central American forearc.

5.2. Isotopic constraints on the plume-contaminated nature of the source

A myriad of studies show the plume-contaminated nature of Central American forearc lavas as the result of emplacement of the CLIP which immediately preceded and instigated subduction initiation (plume-induced subduction initiation, Whattam and Stern (2015a) and references therein). In terms of source components and source mixing, it was shown by Allibon et al. (2008) that the isotopic compositions of Ecuadorian arc or arc-like lava sequences (which according to Whattam and Stern, 2015a are essentially analogous to arc lavas in Sona-Azuero, Golfito and Chagres-Bayano) built upon CLIP oceanic plateau fragments could

be explained in terms of tripolar mixing of three components: a dominant depleted MORB mantle component; a high μ (where μ is $a^{238}U/^{204}Pb$ ratio of an Earth reservoir) component carried by the CLIP; and a subducted pelagic sediment component. It was further shown by Allibon et al. (2008) that an average contribution of 70–75% depleted MORB mantle, 12–15% high μ, and 7–15% pelagic sediments (cherts) is required to explain their composition. Furthermore, Whattam (2018) showed that the Central American lavas in this study also plot within the $^{143}Nd/^{144}Nd$ vs $^{206}Pb/^{204}Pb$ field defined by the Galapagos Plume at 90 Ma similarly to the western Late Cretaceous Ecuadorian lavas in the study of Allibon et al. (2008). It is for these reasons that we use the term 'plume contaminated' to describe the forearc basalts of Sona-Azuero and the VAB of Chagres-Bayano.

5.3. Nature of the contact between "oceanic plateau" and arc and chemotemporal evolution of magmatism

Buchs et al. (2010) present a synthetic 'tectonostratigraphic' chart (their Fig. 3, reproduced in part in our Fig. 10a) but there is a ~10–12 M.y. hiatus between inferred termination of oceanic plateau construction at 85 Ma and incipient arc construction at 75-73 Ma (timing of SI as interpreted by Buchs et al., 2010) at both the Azuero marginal and Golfito complexes. The only study we know of that documents the nature of the contact between the lower "oceanic plateau unit" and the upper arc unit in the Sona-Azuero Complex is that of Corral et al. (2011) (their Fig. 2, reproduced in our Fig. 10b). They (Corral et al., 2011) show a conformable contact between the oceanic plateau basement and the overlying proto-arc sequence, which in turn is conformably overlain by the arc sequence (the Rio Quema Formation, see Fig. 10b). This bolsters the supposition of Whattam and Stern (2015a) of a continuous, uninterrupted magmatic succession between underlying lavas interpreted as plateau and overlying ones interpreted as proto-arc/arc. Lissinna et al. (2006) report that earliest arc activity commenced at 88.3±5 Ma but unfortunately, no further details are available. If earliest formation of the Panamanian Arc was indeed ~90-89 Ma, this supports the model of Whattam and Stern (2015a) that plateau and arc magmatism overlapped beginning about 90 Ma. We also note that Buchs et al. (2010) remark that some earliest supra-subduction zone proto-igneous rocks are indistinguishable from those of 'typical' oceanic plateaus which also hints that plateau and arc magmatism overlapped (or that earliest SI lavas tapped a strongly plume-contaminated source). Corral et al. (2011) provide a stratigraphic section though the Rio Quema Formation (Azuero), showing that the Azuero proto-arc group simply overlies the Azuero (oceanic plateau) igneous basement which, if the ages of Lissinna et al. (2006) are accurate, suggest a continuous, uninterrupted interval from oceanic plateau to proto-arc/arc magmatism. This, coupled with the complete compositional overlap between Sona-Azuero lavas and intrusives interpreted as oceanic plateau and those interpreted as proto-arc and arc suggest that both are related in space and time. Clearly, more stratigraphic and geochronologic investigations are needed but the data in hand support a model whereby the evolution from earlier CLIP-like basalts to younger arc-like lavas was continuous and uninterrupted (Fig. 11a) as opposed to a scenario whereby arc construction occurred upon a pre-existing plateau (Fig. 11b).

It is increasingly clear that the subdivision between oceanic plateau and arc magmatic sequences in Central America are gradational. We recognize that the subdivision is based on lavas and intrusives with negative primitive-mantle normalized high-field strength element anomalies (particularly Nb) being assigned as arc and those without as oceanic plateau. However, it was shown by Whattam and Stern (2011) that the first magmatic expression of some subduction initation systems is MORB-like, and some basalts of lower unit subduction initiation ophiolites exhibit weak primitive mantle normalized negative Nb-anomalies, others do not; a robust negative Nb-anomaly and associated large ion lithophile enrichment is typically seen only in younger lavas and intrusives. We agree with the interpretation of Whattam and Stern (2015a) that the earliest magmatic activity at the Central American Arc system in Panama and Costa Rica was the result of tapping of a hybrid, plume-subduction source as the result of plume-induced subduction initiation. As shown in Sections 5.1.1.-5.1.3, whereas lavas of both Sona-Azuero units - i.e., those interpreted as oceanic plateau and those interpreted as arc - are 'MORB-like', the lavas of the Chagres-Bayano unit are mostly 'arc-like'. We conclude on this basis that magmatism evolved continuously from plume-contaminated MORB- to VAB-like with time consistent with the SIR.

5.4. Subduction initiation mechanisms

As explained by Stern (2004) and later by Stern and Gerya (2018), subduction initiation can be either spontaneous or induced. In the case of the former, there are three possible types: transform collapse, passive margin collapse, and plume head margin collapse (i.e., plume-induced subduction initiation). In contrast, induced subduction initiation is triggered by continued plate convergence following collision, for example of an oceanic plateau with a subduction zone. There are two types of induced subduction initiation: a new subduction zone of similar dip to the original subduction zone can initiate behind the collision (transference) or in front of the collision and (polarity reversal).

The earliest workers to propose spontaneous subduction initiation at a lithospheric weakness (transform separating older, denser lithosphere from younger, warmer lithosphere) was Matsumoto and Tomoda (1983). This idea of spontaneous subduction initiation along a transform fault was adopted by Stern and Bloomer (1992) to explain the early evolution of the Izu Bonin Marianas arc system and by others for other regions of forearc formation (e.g., Whattam et al., 2006, 2008; Shafaii Moghadam et al., 2013; Zhou et al., 2018). Other studies have focused on forced convergence across fracture zones (e.g., Hall et al., 2003). Subduction nucleation along a passive margin (Marques et al., 2014; Ueda et al., 2008; Burov and Cloetingh, 2010; Van der Lee et al., 2008) is implied in the Wilson (1966) cycle but until very recently (Pandey et al., 2019), there are no known Cenozoic examples (Stern, 2004). Pandey et al. (2019) recovered forearc basalts and overlying boninitic-like forearc basalts in the Laxmi Basin, western Indian passive margin, which record geochemical and isotopic attributes identical to first formed lavas of the Izu Bonin Marianas and supra-subduction zone ophiolites and may provide the first evidence for subduction initiation along a passive margin. Perhaps the best example of a induced subduction initiation polarity reversal event is that caused by collision of the Ontong Java Plateau, the world's largest igneous province, which attempted to subduct to the SW at the Vitiaz Trench ~10-4 Ma (Phinney et al., 1999; Cooper and Taylor, 1985). Thick, buoyant lithosphere of the Plateau jammed the subduction zone and caused a subduction polarity flip to the NE. As explained in the Introduction, Buchs et al. (2010) suggested that subduction initiation at the Central American Arc was tectonically induced and resulted from compression of the thickened Caribbean Plate during westward migration of the Americas and collision of the thickened Caribbean Plate with South America. As explained above in Section 5.3, on the basis of a comprehensive set of geochemical, isotopic and geochronologic data and tectonic considerations, we concur with Whattam and Stern (2015a, 2015b) that arc construction in Central America began instead about 90 Ma as the result of plume-induced subduction initiation. A second example of plume-induced subduction initiation has been recently proposed for the Cascadia subduction

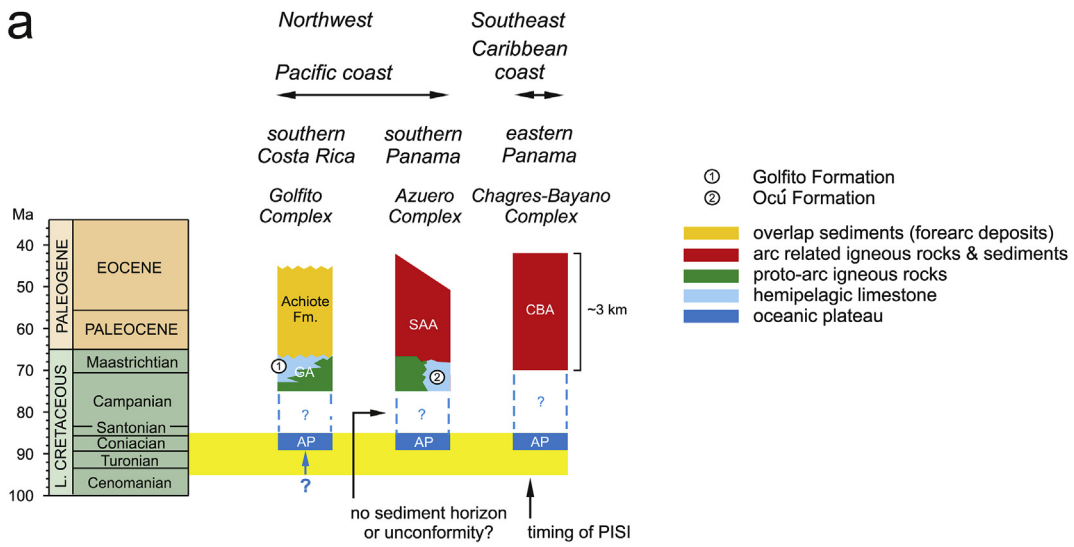

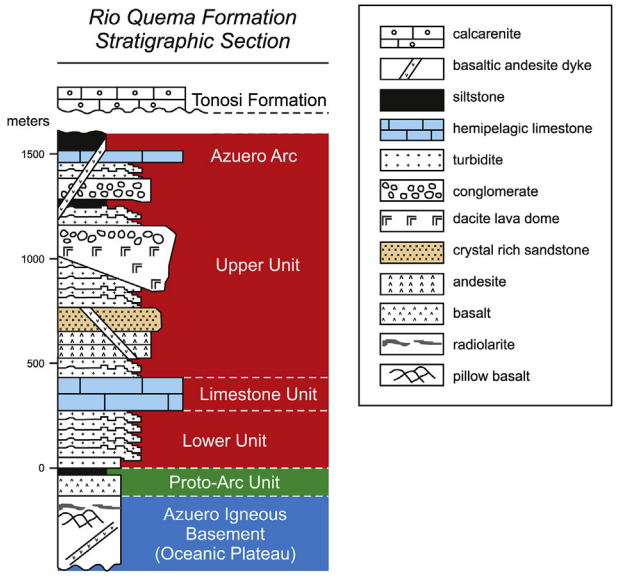

Fig. 10. (a) Chemotemporal relations between the Golfito, Sona-Azuero and Chagres-Bayano as shown on the 'synthetic tectonostratigraphic chart' of Buchs et al. (2010). Unit acronyms (from left to right): AP, Azuero (oceanic) Plateau (89-85 Ma); GA, Golfito Arc (75-66 Ma); SA, Sona-Azuero Arc (75-39 Ma); CBA, Chagres-Bayano Arc (70-39 Ma). (b) Stratigraphy of an Azuero section (the Rio Quema Formation) reproduced from Corral et al. (2011) which provides relations between the Azuero oceanic 'plateau', proto-arc and arc. Other acronyms: PISI, plume-induced subduction initiation. References for ages are provided in Table 1.

zone in the Pacific NW, USA (Stern and Dumitru, 2019) and plume-induced subduction initiation has shown to be viable on the basis of numerical thermomechanical modelling (Gerya et al., 2015).

5.5. Physical nature of the early arc system and tectonic considerations

In their study of Panamanian magmatism circa 75 Ma to present, Wegner et al. (2011) suggest that arc magmatism began in the Sona and Azuero peninsulas at ~71 Ma (Sona-Azuero Arc), then shifted to the Chagres-Bayano region at 66 Ma; Wegner et al. (2011) also apparently consider these as two distinct arcs. We disagree with these notions for several reasons. Firstly, arc lengths are typically not at the 100s of km scale but rather 1000s of km scale. For example, the modern-day Central American Volcanic Arc system is ~1500 km long and the Izu-Bonin Marianas Arc system is ~2800 km

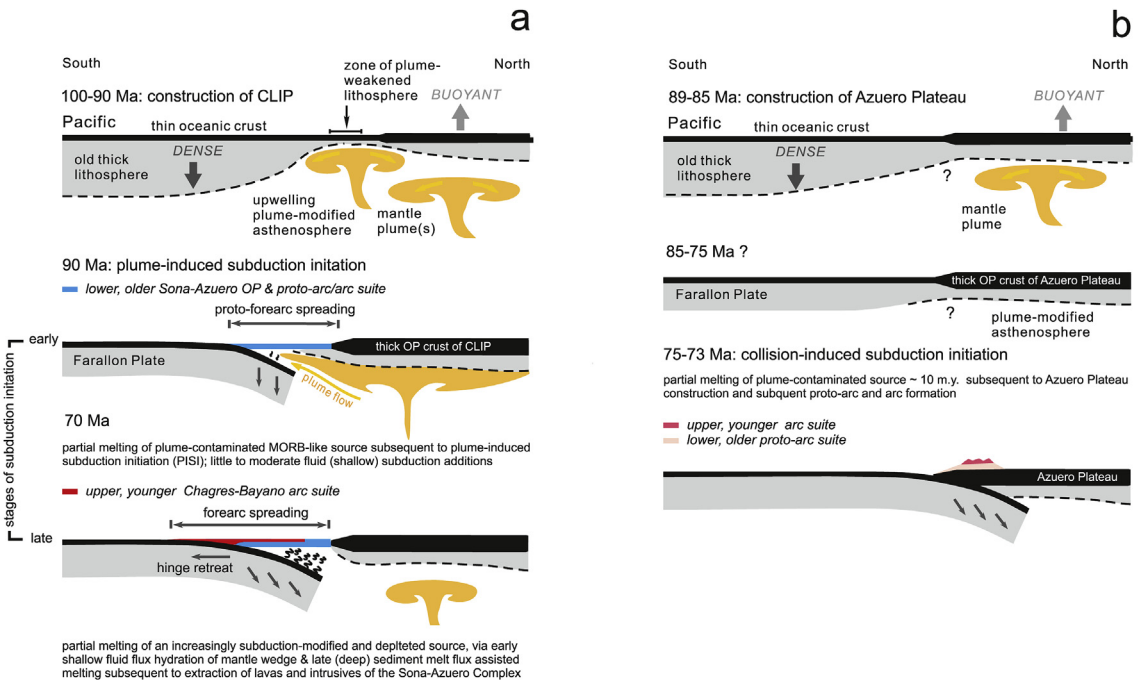

Fig. 11. Two alternative tectonic models to reconcile subduction initiation at the Central American Volcanic Arc system. (a) The earliest stages of subduction initiation were catalyzed by plume emplacement (modified from Whattam and Stern, 2015a). This event began to first form the Sona-Azuero complex which was then followed by incipient formation of the Chagres-Bayano complex, subsequent to slab rollback and hinge retreat. (b) Collision-induced subduction initiation (see Buchs et al., 2010 for details) and subsequent arc construction upon a ~10 m.y. oceanic plateau (based on the ideas of Buchs et al., 2010 and Wegner et al., 2011).

long. The magmatic arc 'belts' along the Sona-Azuero peninsula and the Chagres-Bayano region are only ~200–250 km long, but restoration of paleomagnetically derived vertical-axis rotations (Montes et al., 2012a) suggests that the combined length of the Campanian to Eocene Central American arc was at least 1000 km. Furthermore, combined geochemical and geochronological evidence suggests that the nascent Central American arc stretched westwards from the Nicoya peninsula in western Costa Rica some 200 km south of Nicaragua, to either present-day western Ecuador or Colombia some 1400 km to the east (Whattam and Stern, 2015a). Secondly, the age constraints of Lissinna (2005) indicate that Sona-Azuero magmatic activity was contemporaneous with Chagres-Bayano magmatism between 70 and 40 Ma. Thirdly, unequivocal 'arc' magmatism at the Sona-Azuero and Golfito complexes began by at least 75 Ma (Buchs et al., 2010) but the 89-85 Ma Sona-Azuero CLIP MORB-like oceanic plateau basalts are largely indistinguishable from the younger Sona-Azuero arc and proto-arc basalts. Furthermore, Lissinna et al. (2006) suggest arc magmatism began by ~90 Ma. Finally, as shown by Whattam and Stern (2015a), most (~90-85 Ma) oceanic plateau basalts from the western edge of the CLIP (Costa Rica, e.g., Nicoya, Herradura, Tortugal) including those of Sona-Azuero and the NW segment of the South American Plate in Ecuador and Western Colombia, exhibit subduction modified compositions. Although a lateral west to east transition in chemistry cannot be categorically ruled out, the relations in the chemistry of Sona-Azuero vs. Chagres-Bayano basalts are more consistent with a vertical/stratigraphic transition, although eruptions may have become more arc-like as magmatism retreated from the trench. This chemostratigraphic progression can also be considered as chemotemporal as the change in magmatic affinities is largely vertical and hence a record also of change in chemistry with time; this chemotemporality is identical to that recorded by the slightly older Sona-Azuero and the younger Chagres-Bayano complexes. Thus, we suggest that the Chagres-Bayano arc segment represents a vertical as well as lateral migration of arc magmatism that is also seen for Sona-Azuero circa 71 Ma (Wegner et al., 2011) (Fig. 7). In other words, the Chagres-Bayano arc segment may represent the carapace of the early established Central American Arc system.

If Chagres-Bayano does indeed represent the latest phase of early Central American Arc magmatism, the present position of the Chagres-Bayano arc segment indicates that it is offset to the north. In the tectonic model of Whattam et al. (2012), the early (pre-40 Ma) Central American Arc was shut down at about 40 Ma as the result of collision of an oceanic plateau with the arc system (see also Kerr and Tarney, 2005). As explained by Montes et al. (2012a, 2012b) and Whattam et al. (2012), this collision caused left-lateral offset of the originally contiguous early (pre-40 Ma) Central American Volcanic Arc system which stretched from at least western Costa Rica in the NW to western Ecuador or Colombia in the SE (Whattam and Stern; 2015a) and resulted in a >100 km displacement to the north between 40 and 30 Ma (Lissinna, 2005; Montes et al., 2012a, 2012b). Alternatively, left-lateral offset may have been caused by a shift in the subducted plateau from Azuero to a region to the east (Lissinna et al., 2006) or as the result of collision of South America with the Panamanian Arc system (Farris et al., 2011; Barat et al., 2014). Regardless of the mechanism of displacement or the nature of the colliding body, we suggest that the Chagres-Bayano arc segment was translated to the north after originally forming the carapace and rear of the early arc system subsequent to slab rollback but prior to displacement (Fig. 11).

6. Conclusions

An unambiguous chemotemporal transition from early-formed plume-contaminated MORB-like to VAB-like lavas is seen in Late Cretaceous-Paleogene magmatic arc sequences in Panama as revealed by incompatible trace element compositions which illustrate fundamental differences between the older Sona-Azuero complex and the younger Chagres-Bayano complex. While the

trace element signatures of basalts from both units are similar, the absolute REE concentrations of Chagres-Bayano basalts range to much lower Σ rare earth element concentrations (12–52 ppm) than those of Sona-Azuero (Σ rare earth elements = 33–102 ppm), exhibit more negative high field strength element-anomalies and higher fluid mobile element/immobile element ratios. Relative to Sona-Azuero, the 70-39 Ma Chagres-Bayano basalts reflect higher degrees of partial melting of a more depleted and oxidized mantle source that received greater slab-derived shallow and deep subduction contributions.

Moreover, the Sona-Azuero basalts interpreted as proto-arc and arc are compositionally more similar to the Sona-Azuero basalts interpreted as oceanic plateau than they are to the Chagres-Bayano basalts, which if age estimates are accurate suggest that CAVAS subduction began by ~89 Ma. The overarching chemotemporal trend recorded by Sona-Azuero and Chagres-Bayano sequences may reflect the combined effects of a west to east migration of magmatism at 68 Ma as well as a vertical/stratigraphic transition. We suggest that the arc segment now preserved at Chagres-Bayano was originally generated above and to the rear of Sona-Azuero forearc magmatism and was displaced to the north perhaps due to collision with an oceanic plateau on the Cocos plate, which shut down the early arc system ~40 Ma.

The chemotemporal progression from older MORB-like lavas and intrusives at Sona-Azuero to younger VAB-like lavas at Chagres-Bayano to the east confirms adherence of the Late Cretaceous to Eocene Central American forearc to the SIR, similar to Tethyan ophiolites and the Izu-Bonin-Mariana forearc. Importantly, we note that this adherence is independent of the two competing tectonic models described. In other words, even if arc construction occurred intrusive into and atop a pre-existing oceanic plateau and we exclude the MORB-like affinities of the oceanic plateau, the SIR still applies as the Sona-Azuero Proto-Arc and arc lavas and intrusives are also MORB-like in contrast to those of the Chagres-Bayano Arc which instead exhibit unequivocal volcanic arc affinities.

Acknowledgements

We are grateful to Mark Tupper, NSF EAR-0824299, National Geographic, Smithsonian Institution, and Ricardo Perez S.A. which partially funded this project. S. Zapata and D. Ramirez are acknowledged for their help in the field and for generating the base map with the sample localities. Access to field areas and collection permits were granted by Ministerio de Industria y Comercio of Panamá. We thank Jörg Geldmacher, Jeffrey Ryan, and Yamirka Rojas-Agramonte for their reviews of a previous version of the manuscript and Fernando Marques, Kosuke Ueda and an anonymous reviewer for their reviews of the current manuscript and positive comments which resulted in a greatly improved paper.

Appendix A. Supplementary data

Supplementary data to this article can be found online at https://doi.org/10.1016/j.gr.2019.10.002.

References

Alabaster, T., Pearce, J.A., Malpas, J., 1982. The volcanic stratigraphy and petrogenesis of the Oman ophiolite complex. Contrib. Mineral. Petrol. 81, 168–183.
Allibon, J., Monjoie, P., Lapierre, H., Jaillard, E., Bussy, F., Bosch, D., Senebier, F., 2008. The contribution of the young Cretaceous Caribbean Oceanic Plateau to the genesis of late Cretaceous arc magmatism in the Cordillera Occidental of Ecuador. J. South Am. Earth Sci. 26, 355–368.
Arculus, R.J., and the 29 others of IODP Expedition 351, 2015. A record of subduction initiation 800 in the Izu-Bonin-Mariana arc. Nature Geoscience. https://doi.org/10.1038/ngeo2515.
Barat, F., Mercier de Lépinay, B., Sosson, M., Müller, C., Baumgartner, P., Baumgartner-Mora, C., 2014. Transition from the Farallon Plate subduction to collision between south and Central America: geological evolution of the Panama isthmus. Tectonophysics 622, 145–167.
Bryan, W.B., 1983. Systematics of modal phenocryst assemblages in submarine basalts: Petrologic implications. Contrib. Mineral. Petrol. 83, 62–74.
Buchs, D.M., Arculus, R.J., Baumgartner, P.O., Baumgartner-Mora, C., Ulianov, A., 2010. Late cretaceous arc development on the SW margin of the Caribbean plate: insights from the Golfito, Costa Rica, and Azuero, Panama, complex. Geochem. Geophys. Geosyst. 11 https://doi.org/10.1029/2009GC002901.
Buchs, D.M., Baumgartner, P.O., Baumgartner-Mora, C., Bandini, A.N., Jackett, S.-J., Diserens, M.-O., Stucki, J., 2009. Late Cretaceous to Miocene seamount accretion and mélange formation in the Osa and Burica peninsulas (southern Costa Rica): episodic growth of a convergent margin. In: James, K.H., Lorente, M.A., Pindell, J.L. (Eds.), The Origin and Evolution of the Caribbean Plate, vol. 328. Geological Society Special Publication, pp. 411–456.
Burov, E., Cloetingh, S., 2010. Plume-like upper mantle instabilities drive subduction initiation. Geophys. Res. Lett. 37, L03309. https://doi.org/10.1029/2009GL041535.
Cameron, W.E., 1985. Petrology and origin of primitive lavas from the Trodoos ophiolite, Cyprus. Contrib. Mineral. Petrol. 89, 239–255. https://doi.org/10.1007/BF00379457.
Cooper, P.A., Taylor, B., 1985. Polarity reversal in the Solomon Islands arc. Nature 314, 428–430.
Corral, I., Griera, A., Gómez-Gras, D., Corbella, M., Canals, À., Pineda-Falconett, M., Cardellach, E., 2011. Geology of the cerra Quema Au-Cu deposit (Azuero peninsula, Panama). Geol. Acta 9 (3–4), 481–498, 1 0 . 1 3 4 4/1 0 5 . 0 0 0 0 0 1 7 4 2.
DeBari, S.M., Taylor, B., Spencer, K., Fujioka, K., 1999. A trapped Philippine Sea plate origin for MORB from the inner slope of the Izu-Bonin trench. Earth Planet. Sci. Lett. 174, 183–197.
Dengo, G., 1962. Tectonic-igneous sequence in Costa Rica. In: Engel, A.E.J., James, H.L., Leonard, B.F. (Eds.), Petrologic Studies: A Volume in Honor of A. F. Buddington. Geological Society of America, New York, pp. 133–161.
Di Marco, G., 1994. Les terrains accrétés du Costa Rica: Évolution teconostratigraphique de la marge occidentale de la Plaque Caraïbe. Mem. Geol., vol. 20 Univ. de Lausanne, Lausanne, Switzerland, p. 20.
Di Marco, G., Baumgartner, P.O., Channell, J.E.T., 1995. Late Cretaceous-early Tertiary paleomagnetic data and a revised tectonostratigraphic subdivision of Costa Rica and western Panama. In: Mann, P. (Ed.), Geologic and Tectonic Development of the Caribbean Plate Boundary in Southern Central America, 295, pp. 1–27. Spec. Pap. Geol. Soc. Am.
Dilek, Y., Furnes, H., Shallo, M., 2007. Suprasubduction zone ophiolite formation along the periphery of Mesozoic Gondwana. Gondwana Res. 11, 453–475.
Dilek, Y., Furnes, H., Shallo, M., 2008. Geochemistry of the Jurassic Mirdita Ophiolite (Albania) and the MORB to SSZ evolution of a marginal basin oceanic crust. Lithos 100, 174–209.
Gale, A., Dalton, C.A., Langmuir, C.H., Su, Y., Schilling, J.-G., 2013. The mean composition of ocean ridge basalts. Geochem. Geophys. Geosyst. 14, 489–518. https://doi.org/10.1029/2012GC00433.
Floyd, P.A., Winchester, J.A., 1975. Magma Type and Tectonic Setting Discrimination Using Immobile Elements. Earth and Planetary Science Letters 27, 211–218. https://doi.org/10.1016/0012-821X(75)90031-X.
Gazel, E., Carr, M.J., Hoernle, K., Feigenson, M.D., Hauff, F., Szymanski, D., Van Den Bogaard, P., 2009. The Galapagos-OIB signature in southern Central America: mantle re-fertilization by arc-hotspot interaction. Geochem. Geophys. Geosyst. Q02S11. https://doi.org/10.1029/2008GC002246.
Gazel, E., Hayes, J.L., Hoernle, K., Kelemen, P., Everson, E., Holbrook, W.S., Hauff, F., Van Den Bogaard, P., Vance, E.A., Chu, S., Calvert, A.J., Carr, M.J., Yogodzinski, G.M., 2015. Continental Crust generated in oceanic arcs. Nat. Geosci. 8, 321–327. https://doi.org/10.1038/ngeo2392.
Geldmacher, J., Hanan, B.B., Blichert-Toft, J., Haarp, K., Hoernle, K., Hauff, F., 2001. Hafnium isotope variations in volcanic rocks from the Caribbean Large Igneous Province and Galápagos hotspot tracks. Geochem. Geophys. Geosyst. 4 https://doi.org/10.1029/2002GC000477.
Geldmacher, J., Hoernle, K., Van Den Bogaard, P., Hauff, F., Klügel, A., 2008. Age and geochemistry of the Central American forearc basement (DSDP Leg 67 and 84): insights into Mesozoic arc volcanism and seamount accretion on the fringe of the Caribbean LIP. J. Petrol. 49, 1781–1815. https://doi.org/10.1093/petrology/egn046.
Gerya, T., Stern, R.J., Baes, M., Sobolev, S.V., Whattam, S.A., 2015. Plate tectonics on the Earth triggered by plume-induced subduction initiation. Nature 527, 221–225. https://doi.org/10.1038/nature15752.
Giudice, D., Recchi, G., 1969. Geología del area del projecto minero de Azuero. Ejectora, informe tecnico. Gobierno de la Repub. de Panamá, Panama City, p. 48.
Hall, C.E., Gurnis, Sdrolias, M., Lavier, L.L., Muellar, R.D., 2003. Catastrophic initiation of subduction following forced convergence across fracture zones. Earth Planet. Sci. Lett. 212, 15–30.
Hauff, F., Hoernle, K., Schmincke, H.–U., Werner, R., 1997. A Mid-Cretaceous origin for the Galapagos hotspot: volcanological, petrological and geochemical evidence from Costa Rican oceanic crustal fragments. Geol. Rundsch. 86, 141–155.
Hauff, F., Hoernle, K.A., van den Bogaard, P., Alvarado, G.E., Garbe-Schonberg, D., 2000. Age and geochemistry of basaltic complexes in western Costa Rica: contributions to the geotectonic evolution of Central America. Geochem. Geophys. Geosyst. 1. Paper No. 1999GC000020.
Hawkesworth, C.J., Turner, S.P., McDermott, F., Peate, D.W., van Calsteren, P., 1997. U-Th isotopes in arc magmas: implications for element transfer from the

subducted crust. Science 276, 551–555.
Hoernle, K., van den Bogaard, P., Werner, R., Lissinna, B., Hauff, F., Alvarado, G., Garbe-Schonberg, D., 2002. Missing history (16–71 Ma) of the Galapagos hotspot: implications for the tectonic and biological evolution of the Americas. Geology 30, 795–798. https://doi.org/10.1130/0091-7613(2002).
Ishizuka, O., Kimura, J.-I., Li, Yi B., Stern, R.J., Reagan, M.K., Taylor, R.N., Ohara, Y., Bloomer, S.H., Ishii, T., Hargrove III, U.S., Haraguchi, S., 2006. Early stages in the evolution of the Izu-Bonin arc volcanism: new age, chemical and isotopic constraints. Earth Planet. Sci. Lett. 250, 385–401.
Ishizuka, O., Tani, K., Reagan, M.K., Kanayama, K., Umino, S., Harigane, Y., Sakamoto, I., Miyajima, Y., Yuasa, M., Dunkley, D.J., 2011. The timescales of subduction initiation and subsequent evolution of an oceanic island arc. Earth Planet. Sci. Lett. 306, 229–240.
Kerr, A.C., Tarney, J., 2005. Tectonic evolution of the Caribbean and northwestern South America: The case for accretion of two Late Cretaceous oceanic plateaus. Geology 33, 269–272. https://doi.org/10.1130/G21109.1.
Kerr, A.C., White, R.V., Saunders, A.D., 2000. LIP reading: recognizing oceanic plateaux in the geological record. J. Petrol. 41 (7), 1041–1056.
Kerr, A.C., White, R.V., Thompson, P.M., Tamez, J., Saunders, A.O., 2003. In: Bartolini, C., Bufler, R.T., Blickwede, J. (Eds.), The Circum-Gulf of Mexico and the CaribbeanL Hydrocarbon, Habitats, Basin Formation and Plate Tectonics: American Associate of Petroleum Geologists (MPG) Memoir 79, pp. 126–188.
Kolarsky, R.A., Mann, P., Monechi, S., Meyerhoff, H.D., Pessagno Jr., E.A., 1995. Stratigraphic development of southwestern Panama as determined from integration of marine seismic data and onshore geology. Special Paper. In: Mann, P. (Ed.), Geologic and Tectonic Development of the Caribbean Plate Boundary in Southern Central America, vol. 295. Geological Society of America, pp. 159–200.
Lissinna, B., Hoernle, K., van den Bogaard, P., 2002. Northern migration of arc volcanism in western Panama: evidence for subduction erosion? Eos Transactions, AGU 83, 1463–1464.
Le Bas, M.J., 2000. IUGS reclassification of the high-Mg and picritic volcanic rocks. J. Petrol. 41, 1467–1470.
Lissinna, B., 2005. A Profile Though the Central American Landbridge in Western Panama: 115 Ma Interplay between the Galápagos Hotspot and the Central American Subduction Zone. Ph.D. thesis. Christian-Albrechts University, Kiel, Germany, p. 102.
Lissinna, B., Hoernle, K., Hauff, F., van den Bogaard, P., Sadofsky, S., 2006. The Panamanian island arc and Galápagos hotspot: a case study for the long-term evolution of arc/hotspot interaction. Geophys. Res. Abstr. 8, 05106.
Marques, F.O., Cabral, F.R., Gerya, T.V., Zhu, G., May, D.A., 2014. Subduction initiates at straight passive margins. Geology 42, 331–334. https://doi.org/10.1130/G35246.1.
Matusomoto, T., Tomoda, Y., 1983. Numerical simulation of the initiation of subduction at the fracture. J. Phys. Earth 31, 183–194.
Maury, R.C., Defant, M.J., Bellon, H.,, de Boer, Z.J., Stewart, R.H., Cotten, J., 1995. Early Tertiary arc volcanics from eastern Panama. In: Mann, P. (Ed.), Geologic and Tectonic Development of the Caribbean Plate Boundary in Southern Central America, vol. 295. Specical Paper of the Geological Society of America, pp. 29–34.
Meffre, S., Falloon, T.J., Crawford, T.J., Hoernle, K., Hauff, F., Duncan, R.A., Bloomer, S.H., Wright, D.J., 2012. Basalts erupted along the Tongan fore arc during subduction initiation: evidence from geochronology of dredged rocks from the Tonga fore arc and trench. Geochem. Geophys. Geosyst. 13, Q12003. https://doi.org/10.1029/2012GC004335.
Metti, A., Recchi, G., 1976. Geología de la Peninsula de Soná e Isla de Coiba. In: Memoria Segundo Congreso Latinoamericano de Geología, vol. 2, pp. 541–553 (Sucre, Caracas).
Montes, C., Bayona, G.A., Cardona, A., Buchs, D.M., Silva, C.A., Morón, S., Hoyos, N., Ramírez, D.A., Jaramillo, C.A., Valencia, V., 2012a. Arc-continent collision and orocline formation: closing of the central American seaway. J. Geophys. Res. 117, B04105. https://doi.org/10.1029/2011JB008959.
Montes, C., Cardona, A., McFadden, R., Morón, S.E., Silva, C.A., Restrepo-Morono, S., Ramírez, D.A., Hoyos, N., Wilson, J., Farris, D., Bayona, G.A., Jaramillo, C.A., Valencia, V., Bryan, J., Flores, J.A., 2012b. Evidence for middle Eocene and younger land emergence in central Panama: implications for isthmus closure. Geol. Soc. Am. Bull. https://doi.org/10.1130/B30528.1.
Murton, B.J., M.J., 1989. Tectonic controls on boninite genesis. In: Saunders, A.D. (Ed.), Magmatism in the ocean basins, 43. Geological Society of London Special Publication, pp. 347–377.
Nakamura, N., 1974. Determination of REE, Ba, Fe, Mg, Na and K in carbonaceous and ordinary meteorites. Geochem. Cosmochim. Acta 38, 757–775.
Obando, J.A., 1986. Sedimentología y tectónica del Cretácico y Paleógeno de la region de Golfito, Península de Burica y Península de Osa, Provincia de Puntarenas, Costa Rica. licenciatura thesis. Univ. de Costa Rica, San José, Costa Rica, p. 211. Escuela Centroam. de Geol.
Pandey, D.K., Pandey, A., Whattam, S.A., 2019. Relict subduction initiation along a passive margin in the northwest Indian Ocean. Nat. Commun. 10, 2248. https://doi.org/10.1038/s41467-019-10227-8.
Pearce, J.A., 1983. Role of the subcontinental lithosphere in magma genesis at active continental margins. In: Hawkesworth, C.J., Norry, M.J. (Eds.), Continental Basalts and Mantle Xenoliths, pp. 230–249 (Nantwich, Shiva).
Pearce, J.A., 2003. Supra-subduction zone ophiolites: the search for modern analogues. In: Dilek, Y., Newcomb, S. (Eds.), Ophiolite Concept and the Evolution of Geological Thought, vol. 373. Geological Society of America Special Paper, pp. 269–293.
Pearce, J.A., 2008. Geochemical fingerprinting of oceanic basalts with applications to ophiolite classification and the search for Archean oceanic crust. Lithos 100, 14–48.
Pearce, J.A., Lippard, S.J., Roberts, S., 1984. Characteristics and tectonic significance of supra-subduction zone ophiolites. In: Kokelaar, P., Howels (Eds.), Geology of Marginal Basins, vol. 16. Geological Society of London Special Publication, pp. 77–94.
Pearce, J.A., Norry, N.J., 1979. Petrogenetic implications of Ti, Zr, Y, and Nb variations in volcanic rocks. Contrib. Mineral. Petrol. 69, 33–49.
Pearce, J.A., Robinson, P.T., 2010. The Troodos ophiolitic complex probably formed in a subduction initiation, slab edge setting. Gondwana Res. 18, 60–81.
Phinney, E.J., Mann, P., Coffin, M.F., Shipley, T.H., 1999. Sequence stratigraphy, structure, and tectonic history of the southwestern Ontong Java Plateau adjacent to the North Solomon Trench and Solomon Islands arc. J. Geophys. Res. 104 (B9), 20446–20449.
Pindell, J.L., Kennan, L., 2009. Tectonic evolution of the Gulf of Mexico, Caribbean and northern South America in the mantle reference frame: an update. In: James, K.H., Lorente, M.A., Pindell, J.L. (Eds.), The Origin and Evolution of the Caribbean Plate, vol. 328. Geological Society, London, pp. 1–55.
Reagan, M.K., Ishizuka, O., Stern, R.J., Kelley, K.A., Ohara, Y., Blichert-Toft, J.,, Bloomer, S.–H., Cash, J., Fryer, P., Hanan, B.B., Hickey-Vargas, R., Ishii, T., Kimura, J.I., Peate, D.W., Rowe, M.C., Woods, M., 2010. Fore-arc basalts and subduction initiation in the Izu-Bonin-Mariana system. Geochem. Geophys. Geosyst. 11, Q03X12. https://doi.org/10.1029/2009GC002871.
Reagan, M.K., Pearce, J.A., Petronotis, K., Almeev, R.R., Avery, A.J., Carvallo, C., Chapman, T., Christeson, G.L., Ferré, E.C., Godard, M., Heaton, D.E., Kirchenbaur, M., Kurz, W., Kutterolf, S., Li, H., Li, Y., Mishibayashi, K., Morgan, S., Nelson, W.R., Prytulak, J., Python, M., Robertson, A.H.F., Ryan, J.G., Sager, W.W., Sakuyama, T., Shervais, J.W., Shimizu, K., Whattam, S.A., 2017. Subduction initiation and ophiolite crust: new insights from IODP drilling. Int. Geol. Rev. https://doi.org/10.1080/00206814.2016.1276482.
Robertson, A., 2004. Development of concepts concerning the genesis and emplacement of Tethyan ophiolites in the Eastern Mediterranean and Oman regions. Earth Sci. Rev. 66, 331–387.
Saccani, E., Photiades, A., 2004. Mid-ocean ridge and supra-subduction affinities in the Pindos Massif ophiolites (Greece): implications for magma genesis in a proto-forearc setting. Lithos 73, 229–253.
Schmidt-Effing, R., 1979. Alter und Genese des Nicoya-Komplexes, einer ozeanischen Palaeokruste (Oberjura bis Eozaen) im suedlichen Zentralamerika. Geol. Rundsch. 68, 457–494. https://doi.org/10.1007/BF01820803.
Shafaii Moghadam, H., Corfu, F., Stern, R.J., 2013. U-Pb zircon ages of Late Cretaceous Nain-Dehshir ophiolites, central Iran. J. Geol. Soc. 170, 175–184. https://doi.org/10.1144/jgs2012066.
Shervais, J.W., 1982. Ti-V plots and the petrogenesis of modern and ophiolitic lavas. Earth Planet. Sci. Lett. 59, 110–118.
Shervais, J.W., Reagan, M., Haugen, E., Almeev, R.R., Pearce, J.A., Prytulak, J., Ryan, J.G., Whattam, S.A., Godard, M., Chapman, T., Li, H., Kurz, W., Nelson, W.R., Heaton, D., Kirchenbaur, M., Shimizu, K., Sakuyama, T., Li, Y., Vetter, S.K., 2019. Magmatic response to subduction initiation: Part 1. Fore-Arc basalts of the izu-bonin arc from IODP expedition 352. Geochem. Geophys. Geosyst. 20 https://doi.org/10.1029/2018GC007731.
Sinton, C.W., Duncan, R.A., Denyer, P., 1997. Nicoya Peninsula, Costa Rica: a single suite of Caribbean oceanic plateau magmas. J. Geophys. Res. 102 (15) https://doi.org/10.1029/97JB00681, 507-515,520.
Stern, R.J., 2004. Subduction initiation: spontaneous and induced. Earth Planet. Sci. Lett. 226, 275–292.
Stern, R.J., Bloomer, S.H., 1992. Subduction zone infancy: examples from the Eocene izu–bonin–mariana and jurassic California. Geol. Soc. Am. Bull. 104, 1621–1636.
Stern, R.J., Dumitru, T.A., 2019. Eocene initiation of the Cascadia subduction zone: a second example of plume-induced subduction initiation? Geosphere. https://doi.org/10.1130/GES02050.1.
Stern, R.J., Gerya, T., 2018. Subduction initiation in nature and models: a review. Tectonophysics 746, 173–198.
Sisson, T.W., Grove, T.L., 1993. Experimental investigations of the role of H2O in calc-alkaline differentiation and subduction zone magmatism. Contributions to Mineralogy and Petrology 113, 143–166. https://doi.org/10.1007/BF00283225.
Stern, R.J., Reagan, M., Ishizuka, O., Ohara, Y., Whattam, S., 2012. To understand subduction initiation, study forearc crust: to understand forearc crust, study pphiolites. Lithosphere. https://doi.org/10.1130/L183.1.
Sun, S.S., McDonough, W.F., 1989. Chemical and isotopic systematic of oceanic basalts: implications for mantle composition and processes. In: Saunders, A.D., Norry, M.J. (Eds.), Magmatism in the Ocean Basins, vol. 42. Geological Society of London Special Publication, pp. 313–345.
Tatsumi, Y., Eggins, S., 1995. Subduction Zone Magmatism. Blackwell, London, p. 211.
Tomascak, P.B., Ryan, J.G., Defant, M.J., 2000. Lithium isotope evidence for light element decoupling in the Panama subarc mantle. Geology 28, 507–510.
Torró, L., Proenza, J.A., Marchesi, C., Garcia-Casco, A., Lewis, J.F., 2017. Petrogenesis of meta-volcanic rocks from the maimón formation (Dominican republic): geochemical record of the nascent greater Antilles paleo-arc. Lithos 278–281, 255–273. https://doi.org/10.1016/j.lithos.2017.01.031.
Ueda, K., Gerya, T., Sobolev, S.V., 2008. Subduction initiation by thermal-chemical plumes: numerical studies. Phys. Earth Planet. Inter. 171, 296–312. https://doi.org/10.1016/j.pepi.2008.06.032.
Van der Lee, S., Regenauer-Lieb, K., Yuen, D.A., 2008. The role of water in connecting past and future episodes of subduction. Earth Planet. Sci. Lett. 273, 15–27. https://doi.org/10.1016/j.epsl.2008.04.041.
Wegner, W., Wörner, G., Harmon, R.S., Jicha, B.R., 2011. Magmatic history and

evolution of the Central American land bridge in Panama since Cretaceous times. Geol. Soc. Am. Bull. 123, 703–734.
Whattam, S.A., 2019. Primitive magmas in the early Central American Volcanic Arc system generated by plume-induced subduction initiation. Front. Earth Sci. 6, 114. https://doi.org/10.3389/feart.2018.00114.
Whattam, S.A., Malpas, J., Ali, J.R., Smith, I.E.M., 2008. New SW Pacific tectonic model: cyclical intraoceanic magmatic arc construction and near coeval emplacement along the Australia–Pacific margin in the Cenozoic. Geochem. Geophys. Geosyst. 9 https://doi.org/10.1029/2007GC001710.
Whattam, S.A., Malpas, J., Smith, I.E.M., Ali, J.R., 2006. Link between SSZ ophiolite formation, emplacement and arc inception, Northland New Zealand: U–Pb SHRIMP constraints; Cenozoic SW Pacific tectonic implications. Earth Planet. Sci. Lett. 250, 606–632.
Wörner, G., Harmon, R.S., Hartmann, G., Simon, K., 2005. Igneous geology and geochemistry of the upper Río Chagres basin. In: Singh, V.P., Harmon, R.S. (Eds.), The Río Chagres, Panama: A Multidisciplinary Profile of a Tropical Watershed. Springer, Dordrecht, Netherlands, pp. 65–81.
Whattam, S.A., Montes, C., McFadden, R.R., Cardona, A., Ramirez, D., Valencia, V., 2012. Age and origin of earliest adakitic-like magmatism in Panama: implications for the tectonic evolution of the Panamanian magmatic arc system. Lithos 142–143, 226–244.
Whattam, S.A., Stern, R.J., 2011. The 'subduction initiation rule': a key for linking ophiolites, intra-oceanic forearcs, and subduction initiation. Contrib. Mineral. Petrol. 62, 1031–1045. https://doi.org/10.1007/s00410-011-0638-z.
Whattam, S.A., Stern, R.J., 2015a. Late Cretaceous plume-induced subduction initiation along the southern margin of the Caribbean and NW South America: the first documented example with implications for the onset of plate tectonics. Gondwana Res. 27, 38–63.
Whattam, S.A., Stern, R.J., 2015b. Arc magmatic evolution and the construction of continental crust at the Central American Volcanic Arc system. Int. Geol. Rev. https://doi.org/10.1080/00206814.2015.1103668.
Wilson, J.T., 1966. Did the Atlantic close and re-open? Nature 211, 676–681.
Winchester, J.A., Floyd, P.A., 1977. Geochemical discrimination of different magma series and their differentiation products using immobile elements. Chem. Geol. 20, 325–343.
Wörner, G., Harmon, R.S., Wegner, W., 2009. Geochemical evolution of igneous rocks and changing magma sources during the evolution and closure of the Central American landbridge. In: Kay, S.W., Ramos, V.A., Dickinson, W. (Eds.), Backbone of the Americas: Shallow Subduction, Plateau Uplift and Ridge and Terrane Collision, vol. 204. Geological Society of America Memoir, pp. 183–196.
Zhou, X., Li, Z.-H., Gerya, T.V., Stern, R.J., Xu, Z., Zhang, J., 2018. Subduction initiation dynamics along a transform fault control trench curvature and ophiolite ages. Geology 46, 607–610. https://doi.org/10.1130/G40154.1.